

# The Tenth-Order QED Contribution to the Lepton $g-2$ : Evaluation of Dominant $\alpha^5$ Terms of Muon $g-2$

Toichiro Kinoshita\*

*Laboratory for Elementary-Particle Physics  
Cornell University, Ithaca, New York, 14853*

Makiko Nio†

*Theoretical Physics Laboratory, RIKEN, Wako, Saitama, Japan 351-0198*

(Dated: June 27, 2018)

## Abstract

The QED contribution to the anomalous magnetic moments of electron and muon are known very precisely up to the order  $\alpha^4$ . However, the knowledge of  $\alpha^5$  term will also be required when the precision of measurement improves further. This paper reports the first systematic attempt to evaluate the  $\alpha^5$  term. Feynman diagrams contributing to this term can be classified into six gauge-invariant sets which can be subdivided further into 32 gauge-invariant subsets. Thus far we have numerically evaluated all integrals of 17 gauge-invariant subsets which contain light-by-light-scattering subdiagrams and/or vacuum-polarization subdiagrams. They cover most of leading terms of muon  $g - 2$  and lead to a preliminary result  $663 (20) (\alpha/\pi)^5$ , which is 8.5 times more precise than the old estimate.

PACS numbers: PACS numbers: 13.40.Em, 14.60.Ef, 12.39.Fe, 12.40.Vv

---

\*Electronic address: tk@hep.th.cornell.edu

†Electronic address: nio@riken.jp

## I. INTRODUCTION

The deviation of the electron  $g$  value from 2 predicted by Dirac's theory was first confirmed by an experiment on atomic spectrum [1]. Schwinger showed that this deviation can be explained as the effect of radiative correction by the relativistic renormalized QED which he had developed [2]. Together with the discovery of Lamb shift in the spectrum of hydrogen atom [3], it provided convincing experimental evidence that (until then discredited) QED is capable of predicting the effect of electromagnetic interaction precisely, provided that it is renormalized.

### A. Measurement of electron $g-2$

By 1970's the precision of measurement of electron  $g-2$  was improved by four more orders of magnitude by means of spin precession of the electron moving in a constant uniform magnetic field [4]. The value of the electron  $g-2$  was improved further by three additional orders of magnitude in a Penning trap experiment by Dehmelt's group at the University of Washington. Their published results are [5]

$$\begin{aligned} a_{e-} &= 1\,159\,652\,188.4 (4.3) \times 10^{-12} \quad [3.8 \text{ ppb}], \\ a_{e+} &= 1\,159\,652\,187.9 (4.3) \times 10^{-12} \quad [3.8 \text{ ppb}], \end{aligned} \tag{1}$$

where the numerals 4.3 in parentheses represent the combined statistical and systematic uncertainties in the last digits of the measured value.  $1 \text{ ppb} = 10^{-9}$ .

The precision of measurement has thus been improved by seven orders of magnitude over 40 years. This enormous improvement in measurement was matched by the improvement of theory of radiative correction to the electron  $g-2$  from the order  $\alpha$  to the order  $\alpha^4$ , leading to the most stringent test of the validity of QED.

The uncertainty of the experiment (1) was dominated by the cavity shift due to the interaction of the electron with the hyperboloid cavity, which has a very complicated resonance structure. Several efforts were made to reduce this uncertainty [6, 7]. One of them is to replace the hyperboloid cavity by a cylindrical cavity, which allows analytic computation of the structure of the resonance [8]. Gabrielse's new measurement of the electron  $g-2$  is based on this analysis. Recently a preliminary result of this measurement was reported, which is 7.5 times more precise than (1)[9].

## B. Theory of electron g-2 to order $\alpha^4$

The QED contribution to the electron g-2 can be written as

$$a_e(QED) = A_1 + A_2(m_e/m_\mu) + A_2(m_e/m_\tau) + A_3(m_e/m_\mu, m_e/m_\tau) \quad (2)$$

and  $A_i$ ,  $i = 1, 2, 3$ , can be expanded as

$$A_i = A_i^{(2)} \left(\frac{\alpha}{\pi}\right) + A_i^{(4)} \left(\frac{\alpha}{\pi}\right)^2 + A_i^{(6)} \left(\frac{\alpha}{\pi}\right)^3 + \dots \quad (3)$$

The first four coefficients of  $A_1$  are

$$\begin{aligned} A_1^{(2)} &= 0.5, \\ A_1^{(4)} &= -0.328\,478\,965\dots, \\ A_1^{(6)} &= 1.181\,241\,456\dots, \\ A_1^{(8)} &= -1.728\,3\,(35). \end{aligned} \quad (4)$$

$A_1^{(2)}$  and  $A_1^{(4)}$  are known analytically [2, 10, 11].  $A_1^{(6)}$  was obtained by both numerical [12] and analytic integrations [13].  $A_1^{(8)}$  is obtained thus far by numerical integration only [14]. Its uncertainty has been reduced by 10 compared with the old one [15]. Although it has been evaluated by one method only, it has been subjected to an extensive cross-checking among diagrams of 8th-order and also with 6th-, 4th-, and 2nd-order diagrams.

$A_2$  terms are small:

$$\begin{aligned} A_2^{(4)}(m_e/m_\mu)(\alpha/\pi)^2 &= 2.804 \times 10^{-12}, \\ A_2^{(4)}(m_e/m_\tau)(\alpha/\pi)^2 &= 0.010 \times 10^{-12}, \\ A_2^{(6)}(m_e/m_\mu)(\alpha/\pi)^3 &= -0.924 \times 10^{-13}, \\ A_2^{(6)}(m_e/m_\tau)(\alpha/\pi)^3 &= -0.825 \times 10^{-15} \end{aligned} \quad (5)$$

The contribution of  $A_3$  term is even smaller ( $\sim 2.4 \times 10^{-21}$ ). The non-QED contribution of the Standard Model are also known [16, 17, 18]

$$\begin{aligned} a_e(\text{hadron}) &= 1.671\,(19) \times 10^{-12}, \\ a_e(\text{weak}) &= 0.030\,(1) \times 10^{-12}. \end{aligned} \quad (6)$$

To compare the theory with the measured value of  $a_e$  one needs a value of  $\alpha$  obtained by some non-QED measurement. The best available  $\alpha$  at present is [19, 20]

$$\alpha^{-1}(h/M_{C_s}) = 137.036\,000\,1\,(11) \quad [7.4\,ppb]. \quad (7)$$

This leads to

$$\begin{aligned}
a_e(h/M_{C_s}) &= 1\,159\,652\,175.86\ (0.10)(0.26)(8.48) \times 10^{-12}, \\
a_e(exp) - a_e(h/M_{C_s}) &= 12.4\ (9.5) \times 10^{-12},
\end{aligned}
\tag{8}$$

where 0.10 is the remaining uncertainty of the  $\alpha^4$  term, 0.26 is based on an educated guess ( $A_1^{(10)} = 0(3.8)$ ) made by Mohr and Taylor [20], and 8.48 is the uncertainty in the measurement (7). The error 8.48 is still large but is within a factor 2 of the error of the Seattle measurement (1).

### C. Measurement of muon g-2

The last and best of three measurements of the muon g-2 at CERN had an uncertainty of 7 ppm [21]. After years of hard work the muon g-2 measurement at the Brookhaven National Laboratory has come close to the design goal (0.35 ppm): [22]

$$a_{\mu^-}(exp) = 11\,659\,214\ (8)\ (3) \times 10^{-10} \quad (0.7\ \text{ppm}). \tag{9}$$

The world average of  $a_{\mu}(exp)$  obtained by combining this and earlier measurements [21, 23, 24, 25] is

$$a_{\mu}(exp) = 11\,659\,208\ (6) \times 10^{-10} \quad (0.5\ \text{ppm}). \tag{10}$$

### D. Hadronic and electroweak contributions to muon g-2

Currently, the prediction of the Standard Model reflects the difficulty in the treatment of the hadronic contribution [26, 27, 28, 29, 30, 31]. The lowest-order hadronic vacuum-polarization effect on  $a_{\mu}$  has thus far been determined from three sources,

- (i)  $e^+e^-$  annihilation cross section,
- (ii) hadronic  $\tau$  decays,
- (iii)  $e^+e^- \rightarrow \gamma + \text{hadrons}$  [radiative return].

The process (i) has been analyzed by many groups over years. Some recent results are [32, 33, 34]

$$\begin{aligned}
a_{\mu}(\text{had.LO}) &= 6934\ (53)_{exp}\ (36)_{rad} \times 10^{-11}, \\
a_{\mu}(\text{had.LO}) &= 6924\ (59)_{exp}\ (24)_{rad} \times 10^{-11}, \\
a_{\mu}(\text{had.LO}) &= 6944\ (48)_{exp}\ (10)_{rad} \times 10^{-11}.
\end{aligned}
\tag{11}$$

Recent estimate of hadronic light-by-light scattering contribution is [35]

$$a_\mu(\text{had.NL}) = 136 (25) \times 10^{-11}. \quad (12)$$

The electroweak interaction effect is known to two-loop order: [36, 37]

$$\begin{aligned} a_\mu(\text{weak}) &= 152 (1) \times 10^{-11}, \\ a_\mu(\text{weak}) &= 154 (1) (2) \times 10^{-11}, \end{aligned} \quad (13)$$

where (1) and (2) in the second line are estimates of remaining theoretical uncertainty and Higgs mass uncertainty, respectively.

### E. QED contribution to muon g-2 to order $\alpha^4$

The QED contribution to the muon g-2 can be written as

$$a_\mu(\text{QED}) = A_1 + A_2(m_\mu/m_e) + A_2(m_\tau/m_e) + A_3(m_\mu/m_e, m_\tau/m_e). \quad (14)$$

Renormalizability of QED guarantees that the functions  $A_1$ ,  $A_2$ , and  $A_3$  can be expanded in power series in  $\alpha/\pi$  with finite calculable coefficients:

$$A_i = A_i^{(2)} \left(\frac{\alpha}{\pi}\right) + A_i^{(4)} \left(\frac{\alpha}{\pi}\right)^2 + A_i^{(6)} \left(\frac{\alpha}{\pi}\right)^3 + \dots, \quad i = 1, 2, 3. \quad (15)$$

$A_1$  in (14) is identical with  $A_1$  of (2) and has been evaluated to the eighth (i.e.,  $\alpha^4$ ) order. As for  $A_2$  and  $A_3$ , it is easy to see that  $A_2^{(2)} = A_3^{(2)} = A_3^{(4)} = 0$  since they have no corresponding Feynman diagram.  $A_2^{(4)}$ ,  $A_2^{(6)}$ , and  $A_3^{(6)}$  terms have been evaluated accurately by power series expansion in  $m_e/m_\mu$  or  $m_e/m_\tau$ . Thus far  $A_2^{(8)}$  and  $A_3^{(8)}$  are known mostly by numerical integration.

The QED contribution  $a_\mu(\text{QED})$ , even though it is the predominant term of  $a_\mu$ , has received little attention for many years because of its small error bars. The theoretical uncertainty came predominantly from the  $\alpha^4$  term whose contribution to  $a_\mu$  is about 3.3 ppm. Recently we have completed a new evaluation of the  $\alpha^4$  term in which all contributing terms have been evaluated by two or more independent calculations, uncovering an error in some diagrams [38] and eliminating the  $\alpha^4$  term as a possible source of theoretical uncertainty [38, 39]. This causes the QED contribution shifted to

$$a_\mu(\text{QED}) = 116\,584\,719.43 (0.02)(1.15)(0.85) \times 10^{-11}, \quad (16)$$

where 0.03 is the remaining uncertainty of the  $\alpha^4$  term, an improvement of factor 40 over the previous result [15]. The uncertainty 1.15 comes from a crude estimate of the contribution of the  $\alpha^5$  term, which now stands out as the largest source of uncertainty in  $a_\mu(\text{QED})$ . The error 0.85 comes from the uncertainty in the value of  $\alpha$  given in (7).

The prediction of the Standard Model, including the hadronic vacuum-polarization, hadronic light-by-light contributions, and the electroweak effect, is

$$a_\mu(SM) = 116\,591\,870.7 (76.2) \times 10^{-11}, \quad (17)$$

where the uncertainty in theory is mostly due to the hadronic vacuum-polarization term.

#### **F. Tenth-order term: Why is it needed ?**

A very important byproduct of the study of  $a_e$  is that it gives the best value of the fine structure constant  $\alpha$  available at present. If we use the new experiment by the Harvard group, the precision of  $\alpha$  is almost an order of magnitude better than any other measurement of  $\alpha$ .

Furthermore, the uncertainty of this measurement is only a factor 2 larger than that of theory, which is mostly from the  $\alpha^5$  term, since the  $\alpha^4$  term is known with small error. Thus, when the measurement of  $a_e$  is improved further, reduction of the uncertainty of  $\alpha^5$  term will become crucial in order to obtain a better  $\alpha(a_e)$ .

For the muon the old estimate of  $A_2^{(10)}(m_\mu/m_e)$  was 930 (170), which contributes only 0.054 ppm to  $a_\mu$ , well within the current experimental uncertainty. Thus improving  $A_2^{(10)}(m_\mu/m_e)$  is not urgent. However, it will become an important source of error in the next generation of  $a_\mu$  experiment. This is why it is desirable to obtain a better value of  $A_2^{(10)}(m_\mu/m_e)$ . The preliminary value of  $A_2^{(10)}$  was reported in [40].

## **II. CLASSIFICATION OF TENTH-ORDER DIAGRAMS**

Thus far only a small portion of tenth-order diagrams contributing to the muon g-2 have been evaluated analytically [41], or numerically [42]. Rough estimates based on the renormalization group and other considerations have been made in order to identify leading terms [42, 43, 44, 45].

Of course an enormous amount of work is required to go beyond this and evaluate  $\alpha^5$  terms completely. Fortunately, for the muon  $g-2$  the leading contribution comes from those Feynman diagrams which contain  $\ln(m_\mu/m_e)$  terms whose sources can be readily identified as light-by-light-scattering subdiagrams and vacuum-polarization insertions. Thus relatively modest amount of work will enable us to improve the value of  $A_2^{(10)}(m_\mu/m_e)$  over the previous crude estimate. On the other hand, the electron  $g-2$ , in particular  $A_1^{(10)}$  term, is much harder to evaluate. Besides its gigantic size none of 12672 diagrams is dominant so that every term must be evaluated accurately.

For both  $a_e$  and  $a_\mu$  the first step is to count and classify Feynman diagrams contributing to the  $\alpha^5$  term. The contribution to the mass-independent term  $A_1^{(10)}$  may be classified into six gauge-invariant sets, which further subdivided into 32 gauge-invariant subsets, depending on the nature of subdiagrams (of the vacuum-polarization ( $v-p$ ) type or light-by-light-scattering ( $l-l$ ) type). Classification for  $A_2^{(10)}(m_\mu/m_e)$  follows readily from that of  $A_1^{(10)}$ . With help of the Feynman Diagram auto-generator of GRACE system [47] we count the number of diagrams belonging to each set.

### A. Notation

Vacuum-polarization functions  $\Pi$  needed for the evaluation of the  $\alpha^5$  contribution of the lepton  $g-2$  may be classified as follows: In the following  $\Pi_{x(y)}$  denotes a  $\Pi_x$  containing  $\Pi_y$  on its internal photon line.

$\Pi_2$ , which consists of one closed lepton loop of second-order.

$\Pi_4$ , which consists of three proper lepton loops of fourth order.

$\Pi_{4(2)}$ , which consists of three diagrams of type  $\Pi_4$  in which one  $\Pi_2$  is inserted in the internal photon line.

$\Pi_6$ , which consists of 15 proper sixth-order lepton loops which do not contain v-p loop.

$\Pi_{6(2)}$ , which consists of 30 diagrams of type  $\Pi_6$  in which one  $\Pi_2$  is inserted in the internal photon line.

$\Pi_{4(4)}$ , which consists of 9 diagrams of type  $\Pi_4$  whose internal photon line contains a  $\Pi_4$ .

$\Pi_{4(2,2)}$ , which consists of 3 diagrams of type  $\Pi_4$  whose internal photon line contains two  $\Pi_2$ 's.

$\Pi_8$ , which consists of 105 proper eighth-order lepton loops.

Light-by-light scattering type functions  $\Lambda$  needed for the evaluation of the  $\alpha^5$  contribution of the lepton  $g - 2$  may be classified as follows:

$\Lambda_4$ , which consists of six proper fourth-order lepton loop.

$\Lambda_4^{(2)}$ , which consists of 60 diagrams in which lepton lines and vertices of  $\Lambda_4$  are modified by 2nd-order radiative corrections.

$\Lambda_4^{(4)}$ , which consists of 105 diagrams in which lepton lines and vertices of  $\Lambda_4$  are modified by 4th-order radiative corrections.

$\Lambda_{4(2)}^{(2)}$ , which consists of 60 diagrams in which a v-p diagram  $\Pi_2$  is inserted in the photon line of  $\Lambda_4^{(2)}$ .

$\Lambda_6$ , which consists of 120 proper lepton loops to which 6 photon lines are attached.

Finally we need magnetic moment contributions of various orders.

$M_2$ , which consists of a lepton vertex diagram of second-order.

$M_4$ , which consists of six proper lepton vertices of fourth-order.

$M_6$ , which consists of 50 proper lepton vertices of sixth-order.

$M_{6LL}$ , which consists of 6 sixth-order vertex diagrams containing an *external* light-by-light loop  $\Lambda_4$ .

$M_8$ , which consists of 518 proper lepton vertices of eighth-order which have no closed lepton loops.

$M_{8LLb}$ , obtained by replacing  $\Lambda_4$  by  $\Lambda_4^{(2)}$  in  $M_{6LL}$ , and consists of 60 eighth-order vertex diagrams.

$M_{8LLc}$ , obtained by attaching a virtual photon line to the open muon line in all possible ways, and consists of 48 eighth-order vertex diagrams.

$M_{8LLd}$ , obtained by inserting a  $\Lambda_4$  *internally* in the fourth-order  $M_4$  in all possible ways.



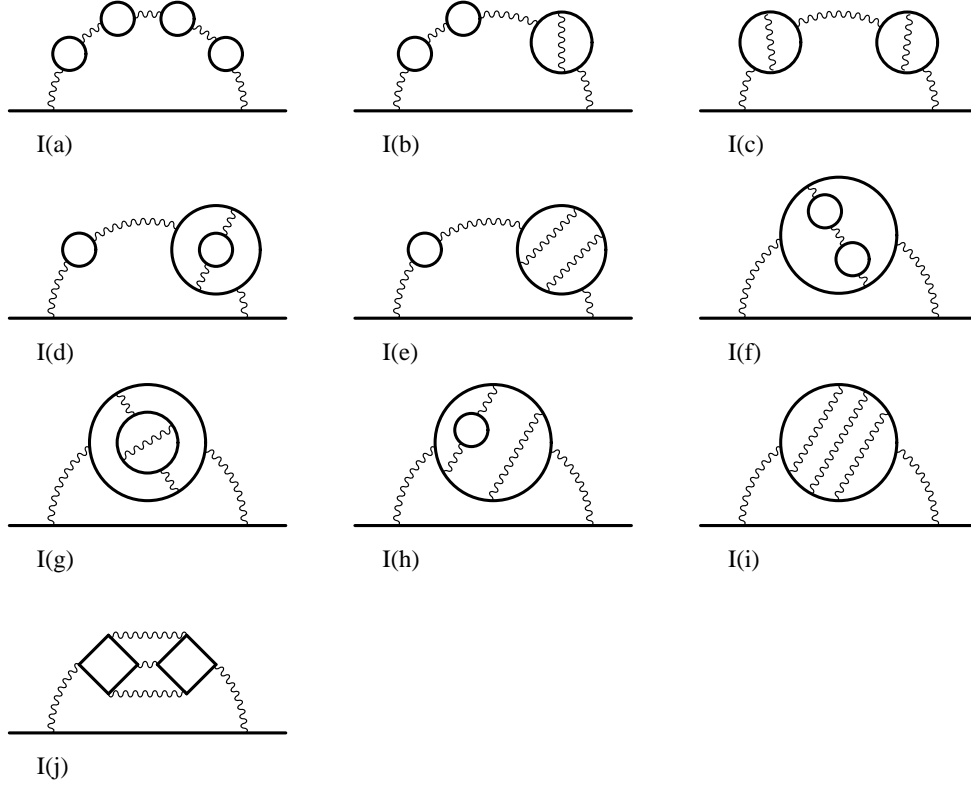


FIG. 1: Set I

## B. Set I

Diagrams of Set I are built from the magnetic moment contribution  $M_2$  of the second-order proper vertex. It consists of 208 Feynman diagrams, which can be classified further into ten gauge-invariant subsets as indicated in Fig. 1. Let us mention only contributions to  $A_1^{(10)}$  and  $A_2^{(10)}$  in this and subsequent sections although many subsets contribute also to  $A_3^{(10)}$ . This is because the contribution of  $A_3^{(10)}$  is negligible compared with others.

*Subset I(a).* Diagrams obtained by inserting four  $\Pi_2$ 's in  $M_2$ . One Feynman diagram belonging to this subset contributes to  $A_1^{(10)}$ . The contribution to  $A_2^{(10)}$  comes from 15 diagrams ( $2^4 - 1 = 15$ ).

*Subset I(b).* Diagrams obtained by inserting two  $\Pi_2$ 's and one  $\Pi_4$  in  $M_2$ . Nine Feynman diagrams of this subset contribute to  $A_1^{(10)}$ . The contribution to  $A_2^{(10)}$  comes from 63 diagrams ( $9(2^3 - 1) = 63$ ).

*Subset I(c).* Diagrams containing two  $\Pi_4$ 's in  $M_2$ . There are nine Feynman diagrams that

contribute to  $A_1^{(10)}$ . The contribution to  $A_2^{(10)}$  comes from 27 diagrams ( $9(2^2 - 1) = 27$ ).

*Subset I(d).* Diagrams obtained by insertion of one  $\Pi_2$  and one  $\Pi_{4(2)}$  in  $M_2$ . Six Feynman diagrams contribute to  $A_1^{(10)}$ . The contribution to  $A_2^{(10)}$  comes from 42 diagrams ( $6(2^3 - 1) = 42$ ).

*Subset I(e).* Diagrams obtained by insertion of one  $\Pi_2$  and one  $\Pi_6$  in  $M_2$ . Thirty Feynman diagrams contribute to  $A_1^{(10)}$ . The contribution to  $A_2^{(10)}$  comes from 90 diagrams ( $30(2^2 - 1) = 90$ ).

*Subset I(f).* Diagrams obtained by insertion of  $\Pi_{4(2,2)}$  in  $M_2$ . The number of diagrams contributing to  $A_1^{(10)}$  is 3. The contribution to  $A_2^{(10)}$  comes from 21 diagrams ( $3(2^3 - 1) = 21$ ).

*Subset I(g).* Diagrams obtained by insertion of  $\Pi_{4(4)}$  in  $M_2$ . The number of diagrams contributing to  $A_1^{(10)}$  is 9. The contribution to  $A_2^{(10)}$  comes from 27 diagrams ( $9(2^2 - 1) = 27$ ).

*Subset I(h).* Diagrams obtained by insertion of  $\Pi_{6(2)}$  in  $M_2$ . The number of diagrams contributing to  $A_1^{(10)}$  is 30. The contribution to  $A_2^{(10)}$  comes from 90 diagrams ( $30(2^2 - 1) = 90$ ).

*Subset I(i).* Diagrams obtained by insertion of  $\Pi_8$  in  $M_2$ . The number of diagrams contributing to  $A_1^{(10)}$  is 105. The contribution to  $A_2^{(10)}$  also comes from 105 diagrams.

*Subset I(j).* Diagrams obtained by insertion of eighth-order photon propagators, which consist of two  $\Lambda_4$ 's with three photons contracted, in  $M_2$ . The number of diagrams contributing to  $A_1^{(10)}$  is 6. The contribution to  $A_2^{(10)}$  comes from 18 diagrams ( $6(2^2 - 1) = 18$ ).

The total number of diagrams of Set I contributing to  $A_1^{(10)}$  is 208. The number of diagrams of Set I contributing to  $A_2^{(10)}$  is 498.

### C. Set II

Diagrams of Set II are built upon six proper fourth-order vertices  $M_4$  by insertion of various closed electron loops. It consists of 600 Feynman diagrams, which can be classified further into six gauge-invariant subsets as indicated in Fig. 2.

*Subset II(a).* Diagrams obtained by inserting three  $\Pi_2$ 's in  $M_4$ . The number of diagrams contributing to  $A_1^{(10)}$  is 24. For the sake of programming convenience this set is subdivided into  $\text{II}(a_1)$ , in which all three  $\Pi_2$ 's are inserted in the same photon line, and  $\text{II}(a_2)$  in which

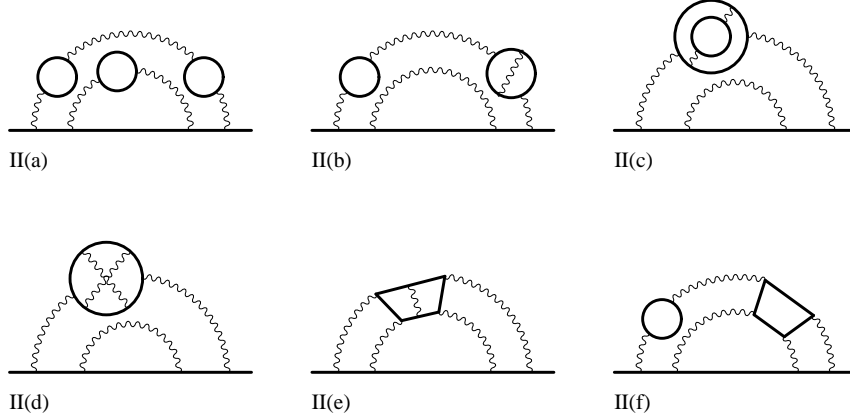


FIG. 2: Set II

$\Pi_2$  are on both photon lines. The total contribution to  $A_2^{(10)}$  comes from 168 diagrams ( $24(2^3 - 1) = 168$ ).

*Subset II(b).* Diagrams obtained by inserting one  $\Pi_2$  and one  $\Pi_4$  in  $M_4$ . The number of diagrams contributing to  $A_1^{(10)}$  is 108. The contribution to  $A_2^{(10)}$  comes from 324 diagrams ( $108(2^2 - 1) = 324$ ).

*Subset II(c).* Diagrams obtained by insertion of  $\Pi_{4(2)}$  in  $M_4$ . The number of diagrams contributing to  $A_1^{(10)}$  is 36. The contribution to  $A_2^{(10)}$  comes from 108 diagrams ( $36(2^2 - 1) = 108$ ).

*Subset II(d).* Diagrams obtained by insertion of  $\Pi_6$  in  $M_4$ . The number of diagrams contributing to  $A_1^{(10)}$  is 180. The contribution to  $A_2^{(10)}$  comes also from 180 diagrams.

*Subset II(e).* Diagrams obtained by insertion of internal light-by-light diagram  $\Lambda_4^{(2)}$  in  $M_4$ . The number of diagrams contributing to  $A_1^{(10)}$  is 180. The contribution to  $A_2^{(10)}$  comes also from 180 diagrams.

*Subset II(f).* Diagrams obtained by insertion of internal light-by-light diagram  $\Lambda_4$  and additional  $\Pi_2$  in  $M_4$ . The number of diagrams contributing to  $A_1^{(10)}$  is 72. The contribution to  $A_2^{(10)}$  comes from 216 diagrams ( $72(2^2 - 1) = 216$ ).

The total number of diagrams of Set II contributing to  $A_1^{(10)}$  is 600. The number of diagrams of Set II contributing to  $A_2^{(10)}$  is 1176.

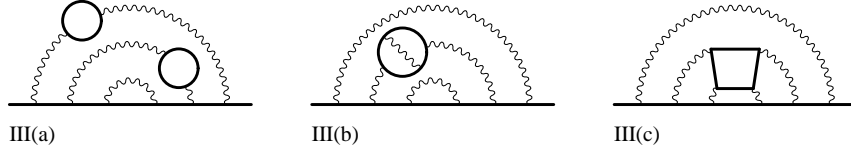


FIG. 3: Set III

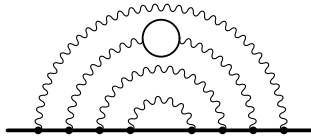


FIG. 4: Set IV

#### D. Set III

Diagrams of Set III are built from 50 proper sixth-order vertices  $M_6$  by insertion of various closed electron loops. This set consists of 1140 Feynman diagrams which can be classified further into three gauge-invariant subsets as indicated in Fig. 3.

*Subset III(a).* Diagrams obtained by inserting two  $\Pi_2$ 's in  $M_6$ . The number of diagrams contributing to  $A_1^{(10)}$  is 300. The contribution to  $A_2^{(10)}$  comes from 900 diagrams ( $300(2^2 - 1) = 900$ ).

*Subset III(b).* Diagrams obtained by inserting  $\Pi_4$  in  $M_6$ . The number of diagrams contributing to  $A_1^{(10)}$  is 450. The contribution to  $A_2^{(10)}$  comes also from 450 diagrams.

*Subset III(c).* Diagrams obtained by insertion of an internal light-by-light diagram  $\Lambda_4$  in  $M_6$ . The number of diagrams contributing to  $A_1^{(10)}$  is 390. The contribution to  $A_2^{(10)}$  comes also from 390 diagrams.

The total number of diagrams of Set III contributing to  $A_1^{(10)}$  is 1140. The number of diagrams of Set II contributing to  $A_2^{(10)}$  is 1740.

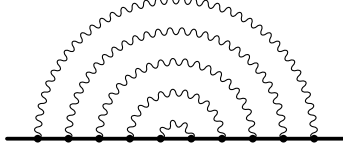


FIG. 5: Set V

### E. Set IV

Set IV is built from 518 proper eighth-order vertices  $M_8$  by inserting a closed lepton loop of second order  $\Pi_2$ . It has only one subset. Total numbers of diagrams of Set IV contributing to  $A_1^{(10)}$  and  $A_2^{(10)}$  are both 2072. A representative diagram is shown in Fig. 4.

### F. Set V

Set V consists of proper tenth-order vertices. It has only one subset consisting of 6354 diagrams and contributes only to  $A_1^{(10)}$ . A representative diagram is shown in Fig. 5.

### G. Set VI

This set consists of vertex diagrams of various orders which contain at least one  $l$ - $l$  subdiagram. Most diagrams of Set VI are built starting from the sixth-order diagram  $M_{6LL}$  which contains an external light-by-light-scattering subdiagram  $\Lambda_4$ . An exception is one subset that contains a subdiagram  $\Lambda_6$ . Note also that diagrams already contained in the sets I, II, and III are excluded. The set VI consists of 2298 Feynman diagrams which can be subdivided into eleven gauge-invariant subsets as indicated in Fig. 6.

*Subset VI(a).* Diagrams obtained by inserting two  $\Pi_2$ 's in the internal photon lines of  $M_{6LL}$ . The number of diagrams contributing to  $A_1^{(10)}$  is 36. The contribution to  $A_2^{(10)}$  comes from 252 diagrams ( $36(2^3 - 1) = 252$ ).

*Subset VI(b).* Diagrams obtained by inserting a  $\Pi_4$  in the internal photon lines of sixth-order diagram  $M_{6LL}$ . The number of diagrams contributing to  $A_1^{(10)}$  is 54. The contribution to  $A_2^{(10)}$  comes from 162 diagrams ( $54(2^2 - 1) = 162$ ).

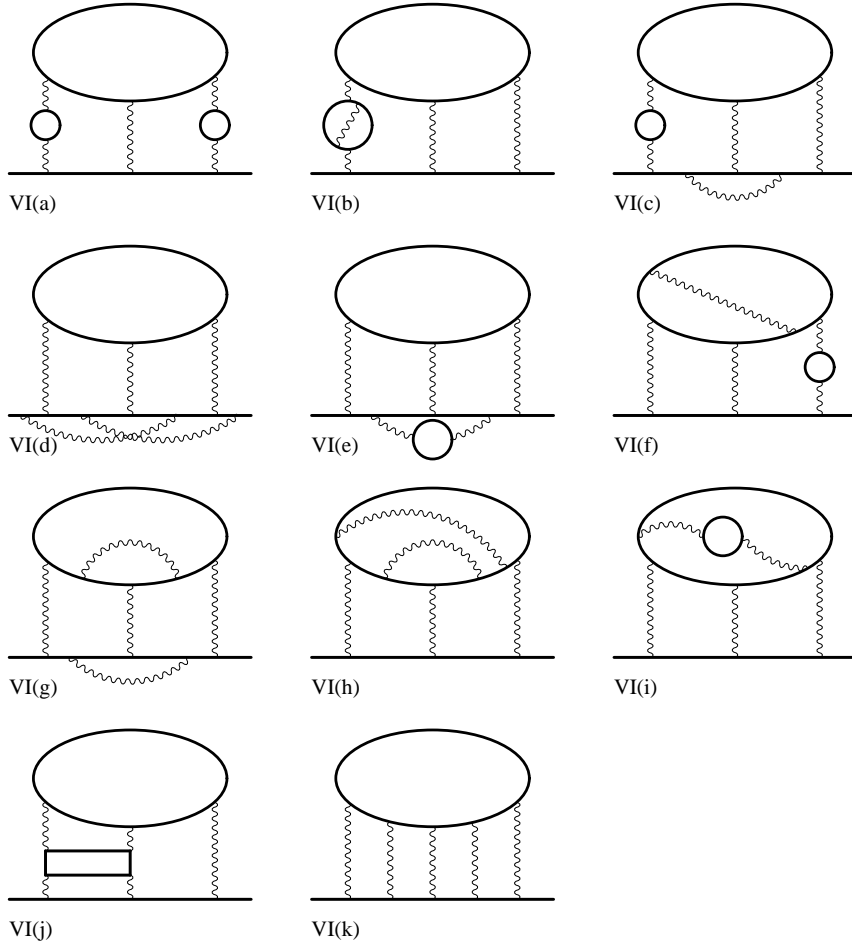


FIG. 6: Set VI

*Subset VI(c).* Diagrams obtained by inserting a  $\Pi_2$  in the photon lines connecting the closed lepton loop  $\Lambda_4$  and the open lepton line in the eighth-order diagrams  $M_{8LLc}$ . The number of diagrams contributing to  $A_1^{(10)}$  is 144. The contribution to  $A_2^{(10)}$  comes from 432 diagrams  $(144(2^2 - 1) = 432)$ .

*Subset VI(d).* This subset consists of diagrams in which the open lepton line of  $M_{6LL}$  is modified by fourth-order radiative corrections. The number of diagrams contributing to  $A_1^{(10)}$  is 492. The contribution to  $A_2^{(10)}$  comes also from 492 diagrams.

*Subset VI(e).* This subset consists of diagrams in which the open lepton line of  $M_{6LL}$  is modified by second-order radiative correction whose photon line has  $\Pi_2$  insertion. The number of diagrams contributing to  $A_1^{(10)}$  is 48. The contribution to  $A_2^{(10)}$  comes from 144 diagrams  $(48(2^2 - 1) = 144)$ .

*Subset VI(f).* This subset is derived from diagrams of  $M_{8LLb}$  in which photon lines connecting  $\Lambda_6$  to the open lepton line receive a  $\Pi_2$  insertion. The number of diagrams contributing to  $A_1^{(10)}$  is 180. The contribution to  $A_2^{(10)}$  comes from 540 diagrams ( $180(2^2 - 1) = 540$ ).

*Subset VI(g).* This subset consists of diagrams in which both the closed loop  $\Lambda_4$  and the open lepton line are modified by second-order radiative corrections. The number of diagrams contributing to  $A_1^{(10)}$  is 480. The contribution to  $A_2^{(10)}$  comes also from 480 diagrams.

*Subset VI(h).* This subset consists of diagrams in which  $\Lambda_4$  is modified by fourth-order radiative corrections. The number of diagrams contributing to  $A_1^{(10)}$  is 630. The contribution to  $A_2^{(10)}$  comes also from 630 diagrams.

*Subset VI(i).* This subset consists of diagrams in which  $\Lambda_4$  is modified by second-order radiative correction whose photon has a  $v.p$  insertion  $\Pi_2$ . The number of diagrams contributing to  $A_1^{(10)}$  is 60. The contribution to  $A_2^{(10)}$  comes from 144 diagrams ( $60(2^2 - 1) = 180$ ).

*Subset VI(j).* This subset is obtained from  $M_{6LL}$  (which contains a  $\Lambda_4$ ) by hanging a second  $\Lambda_4$  on two of three photon lines attached to the open lepton line. The number of diagrams contributing to  $A_1^{(10)}$  is 54. The contribution to  $A_2^{(10)}$  comes from 162 diagrams ( $54(2^2 - 1) = 162$ ).

*Subset VI(k).* This subset consists of vertex diagrams containing  $\Lambda_6$  five of whose photon lines end up on the open lepton line. The number of diagrams contributing to  $A_1^{(10)}$  is 120. The contribution to  $A_2^{(10)}$  comes also from 120 diagrams.

The total number of diagrams of Set VI contributing to  $A_1^{(10)}$  is 2298. The number of diagrams of Set VI contributing to  $A_2^{(10)}$  is 3594.

The total number of Feynman diagrams contributing to  $A_1^{(10)}$  is the sum of contributions from all diagrams described above, which is 12672. The total number for  $A_2^{(10)}$  is 9080.

The number of Feynman diagrams contributing to  $A_3^{(10)}$  can be readily derived from the above result.

### III. LEADING DIAGRAMS CONTRIBUTING TO $a_\mu^{(10)}$

Fortunately, it is not difficult to identify diagrams which may give large contribution to  $a_\mu^{(10)}$ . They are diagrams containing  $\ln(m_\mu/m_e)$  terms which tend to have large numerical values because  $m_\mu$  is much larger than  $m_e$ .

One source of  $\ln(m_\mu/m_e)$  is the vacuum-polarization contribution to the photon propagator which yields the logarithmic factor as a consequence of charge renormalization. The renormalized photon propagator has the form

$$D_R^{\mu,\nu}(q) = -i \frac{g^{\mu\nu}}{q^2} d_R(q^2/m_e^2, \alpha) + \dots, \quad (18)$$

where, to order  $\alpha$ ,

$$d_R(q^2/m_e^2, \alpha) = 1 + \frac{\alpha}{\pi} \left[ \frac{1}{3} \ln(q^2/m_e^2) - \frac{5}{9} + \dots \right]. \quad (19)$$

When  $D_R$  is inserted in  $g-2$  diagrams, the momentum scale is set by the muon mass. Thus the  $\alpha/\pi$  term will give a factor of the order of

$$K_\eta \equiv \frac{2}{3} \ln(\eta(m_\mu/m_e)) - \frac{5}{9}, \quad (20)$$

where  $\eta$  is an fuzzy factor of order 1.  $K_\eta \simeq 3$  for  $\eta = 1$ .

As a matter of fact, more important sources of  $\ln(m_\mu/m_e)$  are diagrams built up from the large sixth-order diagram  $M_{6LL}$  containing an *external* light-by-light scattering subdiagram of closed electron loop  $\Lambda_4$ . (By *external* we mean that one of four photon leg is the external magnetic field. If all photons are virtual photons, we call it *internal*.) The extraordinary size of  $M_{6LL}$  was initially discovered by numerical integration. The primary cause of large size is that it has a logarithmic mass-singularity for  $m_e \rightarrow 0$ . But this is not the whole story. It was pointed out by Yelikhoskii [44] that, in the large  $m_\mu/m_e$  limit, the muon line may be regarded as a static source of Coulomb photons as well as hyperfine spin-spin interaction. Of three photons exchanged between the muon line and the electron loop, one photon is responsible for the spin-spin interaction while the other two are essentially static Coulomb potential. Integration over these Coulomb photon momenta gives a factor  $i\pi$  each, contributing a factor  $\pi^2$  ( $\sim 10$ ) to the leading term

$$M_{6LL}^{(leading)} = \frac{2\pi^2}{3} \ln(m_\mu/m_e). \quad (21)$$

For the physical value of  $m_\mu/m_e$ , this is about 35.  $M_{6LL}$  as a whole is reduced by the negative mass-independent term to about 21, which is still very large. The value of  $M_{6LL}$  containing an electron loop  $\Lambda_4$  is known exactly and its numerical value is [46]

$$M_{6LL} = 20.947\ 924\ 34 \quad (21), \quad (22)$$



where the uncertainty is due to that of the muon mass only.

The difference between  $M_{6LL}$  and  $M_{6LL}^{(leading)}$  may be interpreted as an indicator of the degree to which the picture of static Coulomb potential is valid. One way to incorporate this is to introduce a fudge factor  $\xi$  such that

$$M_{6LL} = \xi^2 M_{6LL}^{(leading)}. \quad (23)$$

In this interpretation we have  $\xi \simeq 0.77$ .

These two sources of  $\ln(m_\mu/m_e)$ , light-light-scattering loop and vacuum-polarization loop, can work together and give even larger numerical factors. For instance, the leading term of the integral  $A_2[VI(a)]$ , which has insertion of two electron loops  $\Pi_2$  and should have been written as VI(a)[e,e,e] following the notation of Table IV, will be of order [42]

$$A_2[VI(a)] \simeq 6K_\eta^2 M_{6LL}, \quad (24)$$

where the factor 6 is the number of ways two electron loops  $\Pi_2$  can be inserted in  $M_{6LL}$ . This leads to  $A_2[VI(a)] \simeq 1130$  for  $\eta = 1$  ( $K_\eta \simeq 3$ ). As is seen later, the actual value is about 543. Thus  $K_\eta \sim 2$ .

Similarly, the subset VI(b), which has insertion of one  $\Pi_4$  in  $M_{6LL}$  (VI(b)[e,e] in the notation of Table IV), will give contribution of the order

$$A_2[VI(b)] \sim 3 \times \frac{3}{4} \times K_\eta M_{6LL} \simeq 142, \quad (25)$$

for  $\eta = 1$  with the help of the identity [43]

$$\Pi_4(k^2) = \frac{\alpha}{\pi} \frac{3}{4} \Pi_2(k^2) + \left(\frac{\alpha}{\pi}\right)^2 k^2 \left(\zeta(3) + \frac{5}{24}\right). \quad (26)$$

The numerical evaluation give  $A_2[VI(b)] \simeq 169$ . Thus  $K_\eta \sim 3.5$  in this case.

If we apply blindly the argument based on (20), we would obtain, for  $K_\eta \sim 3$ ,

$$\begin{aligned} A_2[VI(c)] &\simeq 3K_\eta M_{8LLc} \simeq 27, \\ A_2[VI(e)] &\simeq K_\eta M_{8LLc} \simeq 9, \\ A_2[VI(f)] &\simeq 3K_\eta M_{8LLb} \simeq -4.5, \\ A_2[VI(i)] &\simeq K_\eta M_{8LLb} \simeq -1.5. \end{aligned} \quad (27)$$

Unfortunately, these estimates are completely misleading because  $M_{8LLc}$  is the sum of large terms which tend to cancel each other. Similarly for  $M_{8LLb}$ .

Subsets VI(d), VI(g), and VI(j) have no  $\Pi_2$  insertion and thus will have no particular enhancement although individual members of these subsets (being gauge-dependent) might have rather large values.

Among the diagrams of Sets I - V, the term with the highest power of logarithm is

$$A_2[I(a)] \sim \frac{8}{81} \ln^4(m_\mu/m_e), \quad (28)$$

although its value ( $\sim 80$ ) is not dominating because of its small numerical factor. Actually terms of lower logarithmic powers reduce this to an even smaller value ( $\sim 20$ ).

In the study of eighth-order terms, the value of  $K_\eta$  was found to be smaller than 3 in most cases and varies in the range  $2 < K_\eta < 2.5$ , except for VI(b). Thus the estimates given above for  $\eta = 1$  (or  $K_\eta \sim 3$ ) are likely to be overestimates by  $20 \sim 50\%$ .

The contribution of the subset VI(k) had been estimated in a different manner. It is shown [44] that the leading term in the large  $m_\mu/m_e$  limit is of the form

$$A_2[VI(k)] = \pi^4(0.438.. \ln(m_\mu/m_e) + \dots). \quad (29)$$

Based on this observation it was estimated that [43]

$$A_2[VI(k)] \simeq 185 \pm 85. \quad (30)$$

This term is large mainly because of the presence of the  $\pi^4$  factor. Its origin can be readily understood by a generalization of the argument leading to Eq. (21) to the case in which  $2n+1$  photons are exchanged between the light-by-light type loop  $\Lambda_{2n+2}$ ,  $n=1,2,\dots$ , and the muon line [44]. In the large  $m_\mu/m_e$  limit this mechanism generates the structure

$$A_2^{(2n+1)} \simeq c_n \pi^{2n} \ln(m_\mu/m_e) + \dots. \quad (31)$$

Numerical values of some  $c_n$  are known [48]

$$\begin{aligned} c_1 &= \frac{2}{3}, \\ c_2 &= 0.438\dots \end{aligned} \quad (32)$$

#### IV. ANALYTICALLY KNOWN CONTRIBUTION TO $a_\mu^{(10)}$

At present only a small number of integrals in the subsets I(a), I(b), I(c), II(a), and II(b) are known analytically. Their expansion in the ratio  $m_e/m_\mu$  are given in [41]. From Table

2 of [41] we obtain

$$\begin{aligned}
a_\mu[I(a)] &= 22.566\,973 \text{ (3)}, \\
a_\mu[I(b)] &= 30.667\,091 \text{ (3)}, \\
a_\mu[I(c)] &= 5.141\,395 \text{ (1)}, \\
a_\mu[II(a)] &= -36.174\,859 \text{ (2)}, \\
a_\mu[II(b)] &= -23.462\,173 \text{ (1)},
\end{aligned} \tag{33}$$

where the uncertainties come from the measurement uncertainty of  $m_e/m_\mu$  only. These results show strong cancellation among diagrams of Sets I and II, which is analogous with the cancellation among Group I and Group II diagrams contributing to the eighth-order term of muon g-2.

## V. NUMERICAL EVALUATION OF DIAGRAMS CONTRIBUTING TO $a_\mu^{(10)}$

As was discussed in Section II diagrams containing light-by-light-scattering subdiagrams, namely the Set VI, is the source of dominant contribution to  $a_\mu^{(10)}$ . However, let us describe the results of numerical evaluation starting from the Set I.

### A. Set I

Integrals for the diagrams of Set I, except for subsets I(i) and I(j), can be readily obtained from eighth-order diagrams belonging to Group I by insertion of  $v$ - $p$  loops. Diagrams numerically evaluated thus far are shown in Tables I, II and III. Summing up the first four lines of Table I one obtains

$$\begin{aligned}
A_2[I(a)] &= M_{2,p2:4}^{(e,e,e,e)} + M_{2,p2:4}^{(e,e,e,m)} + M_{2,p2:4}^{(e,e,m,m)} + M_{2,p2:4}^{(e,m,m,m)} \\
&= 22.567\,05 \text{ (25)}.
\end{aligned} \tag{34}$$

Similarly, we find from the rest of Table I

$$\begin{aligned}
A_2[I(b)] &= M_{2,p4,p2:2}^{(e,e,e)} + M_{2,p4,p2:2}^{(e,m,e)} + M_{2,p4,p2:2}^{(e,m,m)} + M_{2,p4,p2:2}^{(m,e,e)} + M_{2,p4,p2:2}^{(m,m,e)} \\
&= 30.667\,54 \text{ (33)}, \\
A_2[I(c)] &= M_{2,p4:2}^{(e,e)} + M_{2,p4:2}^{(e,m)} \\
&= 5.141\,38 \text{ (15)},
\end{aligned} \tag{35}$$

The values of  $A_2[I(a)]$ ,  $A_2[I(b)]$ , and  $A_2[I(c)]$  are in good agreement with semi-analytic values [41] quoted in (33).

$A_2[I(d)]$  is evaluated from the entries in Table II together with Table III and Table VI of [39], which list residual renormalization terms. We obtain

$$\begin{aligned}
M_{2,p4(p2)p2}^{(e(e),e)} &= 2M_{2,p4A(p2)p2}^{(e(e),e)} + 4M_{2,p4B(p2)p2}^{(e(e),e)} - 4\Delta B_{2,p2}^{(e,e)} M_{2,p2:2}^{(m,e,e)} \\
&= 7.45173 \quad (101), \\
M_{2,p4(p2)p2}^{(m(e),e)} &= 2M_{2,p4A(p2)p2}^{(m(e),e)} + 4M_{2,p4B(p2)p2}^{(m(e),e)} - 4\Delta B_{2,p2}^{(m,e)} M_{2,p2:2}^{(m,m,e)} \\
&= 1.02576 \quad (12), \\
M_{2,p4(p2)p2}^{(e(m),e)} &= 2M_{2,p4A(p2)p2}^{(e(m),e)} + 4M_{2,p4B(p2)p2}^{(e(m),e)} - 4\Delta B_{2,p2}^{(e,m)} M_{2,p2:2}^{(m,e,e)} \\
&= 0.13084 \quad (2), \\
M_{2,p4(p2)p2}^{(m(m),e)} &= 2M_{2,p4A(p2)p2}^{(m(m),e)} + 4M_{2,p4B(p2)p2}^{(m(m),e)} - 4\Delta B_{2,p2}^{(m,m)} M_{2,p2:2}^{(m,m,e)} \\
&= 7.17353 \quad (81) \times 10^{-2}, \tag{36}
\end{aligned}$$

$$\begin{aligned}
M_{2,p4(p2)p2}^{(e(e),m)} &= 2M_{2,p4A(p2)p2}^{(e(e),m)} + 4M_{2,p4B(p2)p2}^{(e(e),m)} - 4\Delta B_{2,p2}^{(e,e)} M_{2,p2:2}^{(m,m,e)} \\
&= 0.15845 \quad (3), \\
M_{2,p4(p2)p2}^{(m(e),m)} &= 2M_{2,p4A(p2)p2}^{(m(e),m)} + 4M_{2,p4B(p2)p2}^{(m(e),m)} - 4\Delta B_{2,p2}^{(m,e)} M_{2,p2:2}^{(m,m,m)} \\
&= 4.82662 \quad (1) \times 10^{-2}, \\
M_{2,p4(p2)p2}^{(e(m),m)} &= 2M_{2,p4A(p2)p2}^{(e(m),m)} + 4M_{2,p4B(p2)p2}^{(e(m),m)} - 4\Delta B_{2,p2}^{(e,m)} M_{2,p2:2}^{(m,e,m)} \\
&= 5.29020 \quad (63) \times 10^{-3}, \tag{37}
\end{aligned}$$

From these contributions we obtain  $A_2[I(d)]$ :

$$\begin{aligned}
A_2[I(d)] &= M_{2,p4(p2)p2}^{(e(e),e)} + M_{2,p4(p2)p2}^{(m(e),e)} + M_{2,p4(p2)p2}^{(e(m),e)} + M_{2,p4(p2)p2}^{(m(m),e)} \\
&\quad + M_{2,p4(p2)p2}^{(e(e),m)} + M_{2,p4(p2)p2}^{(m(e),m)} + M_{2,p4(p2)p2}^{(e(m),m)} \\
&= 8.89207 \quad (102). \tag{38}
\end{aligned}$$

Several terms of  $A_2[I(d)]$  was also evaluated by an alternative method using an exact spectral function of  $\Pi_4(\Pi_2)$  in which two loop masses are equal. They are listed at the bottom of Table II. They are in good agreement with the values given in (36) and (37).

$A_2[I(e)]$  is evaluated using the Padé approximant for  $\Pi_6$ , which is known to be a very good approximation from an earlier work. Our result is

$$\begin{aligned}
A_2[I(e)] &= M_{2,p6p2}^{(e,e)} + M_{2,p6p2}^{(e,m)} + M_{2,p6p2}^{(m,e)} \\
&= -1.219\ 20\ (71).
\end{aligned} \tag{39}$$

$A_2[I(f)]$  is evaluated using the entries of Table III together with Table VI. We obtain

$$\begin{aligned}
a_{2,p4(p2:2)}^{(m,e(e,e))} &= \Delta M_{2,p4A(p2:2)}^{(m,e(e,e))} + \Delta M_{2,p4B(p2:2)}^{(m,e(e,e))} - 2\Delta B_{2,p2:2}^{(e(e,e))} M_{2,p2}^{(m,e)} \\
&= 2.88598\ (9), \\
a_{2,p4(p2:2)}^{(m,e(e,m))} &= \Delta M_{2,p4A(p2:2)}^{(m,e(e,m))} + \Delta M_{2,p4B(p2:2)}^{(m,e(e,m))} - 2\Delta B_{2,p2:2}^{(e(e,m))} M_{2,p2}^{(m,e)} \\
&= 0.16111\ (3), \\
a_{2,p4(p2:2)}^{(m,e(m,m))} &= \Delta M_{2,p4A(p2:2)}^{(m,e(m,m))} + \Delta M_{2,p4B(p2:2)}^{(m,e(m,m))} - 2\Delta B_{2,p2:2}^{(e(m,m))} M_{2,p2}^{(m,e)} \\
&= 0.01063\ (1), \\
a_{2,p4(p2:2)}^{(m,m(e,e))} &= \Delta M_{2,p4A(p2:2)}^{(m,m(e,e))} + \Delta M_{2,p4B(p2:2)}^{(m,m(e,e))} - 2\Delta B_{2,p2:2}^{(m(e,e))} M_{2,p2}^{(m,m)} \\
&= 0.53660\ (9), \\
a_{2,p4(p2:2)}^{(m,m(e,m))} &= \Delta M_{2,p4A(p2:2)}^{(m,m(e,m))} + \Delta M_{2,p4B(p2:2)}^{(m,m(e,m))} - 2\Delta B_{2,p2:2}^{(m(e,m))} M_{2,p2}^{(m,m)} \\
&= 0.09079\ (2),
\end{aligned} \tag{40}$$

From these contributions we obtain  $A_2[I(f)]$ :

$$\begin{aligned}
A_2[I(f)] &= a_{2,p4(p2:2)}^{(m,e(e,e))} + a_{2,p4(p2:2)}^{(m,e(e,m))} + a_{2,p4(p2:2)}^{(m,e(m,m))} + a_{2,p4(p2:2)}^{(m,m(e,e))} + a_{2,p4(p2:2)}^{(m,m(e,m))} \\
&= 3.68510\ (13).
\end{aligned} \tag{41}$$

## B. Set II

Integrals of Set II, except for subset II(e), can be readily obtained from eighth-order diagrams belonging to Group II by insertion of  $v$ - $p$  loops. We have evaluated only subsets II(a), II(b), and II(f) thus far. From Table IV and Table VI of this paper and Tables III

and VI of [39], we obtain

$$\begin{aligned} M_{4,p2:3}^{(e,e,e)} &= 2M_{4a,p2:3}^{(e,e,e)} + M_{4b,p2:3}^{(e,e,e)\alpha} + M_{4b,p2:3}^{(e,e,e)\beta} - \Delta B_2 M_{2,p2:3}^{(e,e,e)} - \Delta B_{2,p2:3}^{(e,e,e)} M_2 \\ &= -28.43132 \quad (344), \end{aligned}$$

$$\begin{aligned} M_{4,p2:2,p2}^{(e,e)(e)} &= 2M_{4a,p2:2,p2}^{(e,e)(e)} + M_{4b,p2:2,p2}^{(e,e)(e)} + M_{4b,p2,p2:2}^{(e)(e,e)} - \Delta B_{2,p2}^{(e)} M_{2,p2:2}^{(e,e)} - \Delta B_{2,p2:2}^{(e,e)} M_{2,p2}^{(e)} \\ &= -27.42432 \quad (127), \end{aligned}$$

$$\begin{aligned} M_{4,p2:3}^{(e,e,m)} &= 2M_{4a,p2:3}^{(e,e,m)\emptyset} + M_{4b,p2:3}^{(e,e,m)\emptyset} + M_{4b,p2:3}^{(\emptyset)(e,e,m)} - \Delta B_2 M_{2,p2:3}^{(e,e,m)} - \Delta B_{2,p2:3}^{(e,e,m)} M_2 \\ &= -6.79245 \quad (56), \end{aligned}$$

$$\begin{aligned} M_{4,p2:2,p2}^{(e,e)(m)} &= 2M_{4a,p2:2,p2}^{(e,e)(m)} + M_{4b,p2:2,p2}^{(e,e)(m)} + M_{4b,p2,p2:2}^{(m)(e,e)} - \Delta B_{2,p2}^{(m)} M_{2,p2:2}^{(e,e)} - \Delta B_{2,p2:2}^{(e,e)} M_{2,p2}^{(m)} \\ &= -1.95703 \quad (37), \end{aligned} \tag{42}$$

$$\begin{aligned} M_{4,p2:2,p2}^{(e,m)(e)} &= 4M_{4a,p2:2,p2}^{(e,m)(e)} + 2M_{4b,p2:2,p2}^{(e,m)(e)} + 2M_{4b,p2,p2:2}^{(e)(e,m)} - 2\Delta B_{2,p2}^{(e)} M_{2,p2:2}^{(e,m)} - 2\Delta B_{2,p2:2}^{(e,m)} M_{2,p2}^{(e)} \\ &= -4.14893 \quad (48), \end{aligned}$$

$$\begin{aligned} M_{4,p2:3}^{(e,m,m)} &= 2M_{4a,p2:3}^{(e,m,m)} + M_{4b,p2:3}^{(e,m,m)\emptyset} + M_{4b,p2:3}^{(\emptyset)(e,m,m)} - \Delta B_2 M_{2,p2:3}^{(e,m,m)} - \Delta B_{2,p2:3}^{(e,m,m)} M_2 \\ &= -0.95284 \quad (14), \end{aligned}$$

$$\begin{aligned} M_{4,p2:2,p2}^{(m,m)(e)} &= 2M_{4a,p2:2,p2}^{(m,m)(e)} + M_{4b,p2:2,p2}^{(m,m)(e)} + M_{4b,p2,p2:2}^{(e)(m,m)} - \Delta B_{2,p2}^{(e)} M_{2,p2:2}^{(m,m)} - \Delta B_{2,p2:2}^{(m,m)} M_{2,p2}^{(e)} \\ &= -0.28902 \quad (29), \end{aligned}$$

$$\begin{aligned} M_{4,p2:2,p2}^{(e,m)(m)} &= 4M_{4a,p2:2,p2}^{(e,m)(m)} + 2M_{4b,p2:2,p2}^{(e,m)(m)} + 2M_{4b,p2,p2:2}^{(m)(e,m)} - 2\Delta B_{2,p2}^{(m)} M_{2,p2:2}^{(e,m)} - 2\Delta B_{2,p2:2}^{(e,m)} M_{2,p2}^{(m)} \\ &= -0.47576 \quad (23). \end{aligned} \tag{43}$$

Adding up these contributions one obtains

$$A_2[II(a)] = -70.4717 \quad (38). \tag{44}$$

From Table V and Table VI of this paper and Tables III and VI of [39] we obtain

$$\begin{aligned}
M_{4,p4p2}^{(e,e)} &= 2\Delta_1 M_{4a,p4p2}^{(e,e)\langle\rangle} + \Delta_1 M_{4b,p4p2}^{(e,e)\langle\rangle} + \Delta_1 M_{4b,p4p2}^{\langle\rangle(e,e)} + (p4 \leftrightarrow p2) \\
&\quad - \Delta B_2 M_{2,p4p2}^{(e,e)} - \Delta B_{2,p4p2}^{(e,e)} M_2 \\
&= -19.04191 \quad (203), \\
M_{4,p4p2}^{(e,m)} &= 2\Delta_1 M_{4a,p4p2}^{(e,m)\langle\rangle} + \Delta_1 M_{4b,p4p2}^{(e,m)\langle\rangle} + \Delta_1 M_{4b,p4p2}^{\langle\rangle(e,m)} + (p4 \leftrightarrow p2) \\
&\quad - \Delta B_2 M_{2,p4p2}^{(e,m)} - \Delta B_{2,p4p2}^{(e,m)} M_2 \\
&= -1.28845 \quad (25), \\
M_{4,p4p2}^{(m,e)} &= 2\Delta_1 M_{4a,p4p2}^{(m,e)\langle\rangle} + \Delta_1 M_{4b,p4p2}^{(m,e)\langle\rangle} + \Delta_1 M_{4b,p4p2}^{\langle\rangle(m,e)} + (p4 \leftrightarrow p2) \\
&\quad - \Delta B_2 M_{2,p4p2}^{(m,e)} - \Delta B_{2,p4p2}^{(m,e)} M_2 \\
&= -3.13132 \quad (25), \tag{45}
\end{aligned}$$

$$\begin{aligned}
M_{4,p4p2}^{(e)(e)} &= 2\Delta_2 M_{4a,p4p2}^{(e)(e)} + \Delta_2 M_{4b,p4p2}^{(e)(e)} + (p4 \leftrightarrow p2) \\
&\quad - \Delta B_{2,p2}^{(e)} M_{2,p4}^{(e)} - \Delta B_{2,p4}^{(e)} M_{2,p2}^{(e)} \\
&= -9.42667 \quad (145), \\
M_{4,p4p2}^{(e)(m)} &= 2\Delta_2 M_{4a,p4p2}^{(e)(m)} + \Delta_2 M_{4b,p4p2}^{(e)(m)} + (p4 \leftrightarrow p2) \\
&\quad - \Delta B_{2,p2}^{(m)} M_{2,p4}^{(e)} - \Delta B_{2,p4}^{(e)} M_{2,p2}^{(m)} \\
&= -0.60877 \quad (18), \\
M_{4,p4p2}^{(m)(e)} &= 2\Delta_2 M_{4a,p4p2}^{(m)(e)} + \Delta_2 M_{4b,p4p2}^{(m)(e)} + (p4 \leftrightarrow p2) \\
&\quad - \Delta B_{2,p2}^{(e)} M_{2,p4}^{(m)} - \Delta B_{2,p4}^{(m)} M_{2,p2}^{(e)} \\
&= -1.27436 \quad (27). \tag{46}
\end{aligned}$$

Adding up these values we obtain

$$A_2[II(b)] = -34.7715 \quad (26). \tag{47}$$

Table VII lists numerical results of set II(f) obtained in Version A. The results obtained by an alternate formulation (Version B) are listed in Table VIII. Combining the values in these tables statistically one obtains

$$\begin{aligned}
A_2[II(f)]^{(e,e)} &= -57.0633(109), \\
A_2[II(f)]^{(e,m)} &= -4.7157(31), \\
A_2[II(f)]^{(m,e)} &= -15.6857(37). \tag{48}
\end{aligned}$$

From (48) one obtains

$$A_2[II(f)] = -77.4648(120). \quad (49)$$

### C. Set VI

By far the largest contribution to  $A_2^{(10)}$  comes from the subset VI(a), followed by the subset VI(b). Their integrals can be readily obtained by insertion of v-p functions  $\Pi_2$  and  $\Pi_4$  into the sixth-order diagram  $M_{6LL}$ . We have evaluated them precisely by VEGAS. The results are listed in Table IX. Summing them up, we obtain

$$A_2[VI(a)] = 629.1407 \quad (118), \quad (50)$$

and

$$A_2[VI(b)] = 181.1285 \quad (51). \quad (51)$$

The difference between VI(a)[e,e,e] of Table IX and old one in Eq.(2.49) of [42] is due to a program error in the latter. The results in Table IX show that the leading term estimate (24) is an overestimate by a factor two, while the estimate (25) is not too far off.

Contributions of subsets VI(c), VI(e), VI(f) and VI(i) are also not difficult to evaluate, since they can be readily obtained by insertion of  $\Pi_2$  into some eighth-order integrals. Their numerical values are listed in Tables X, XI, XII, and XIII. From this we obtain

$$\begin{aligned} A_2[VI(c)]^{(e,e)} &= \Delta M_{8LLEp}^{(e,e)} + \Delta M_{8LLFp}^{(e,e)} + \Delta M_{8LLGp}^{(e,e)} + \Delta M_{8LLHp}^{(e,e)} + \Delta M_{8LLIp}^{(e,e)} - 2\Delta B_2 M_{6LLp}^{(e,e)} \\ &= -17.0505 \quad (1122), \\ A_2[VI(c)]^{(m,e)} &= \Delta M_{8LLEp}^{(m,e)} + \Delta M_{8LLFp}^{(m,e)} + \Delta M_{8LLGp}^{(m,e)} + \Delta M_{8LLHp}^{(m,e)} + \Delta M_{8LLIp}^{(m,e)} - 2\Delta B_2 M_{6LLp}^{(m,e)} \\ &= -14.2744 \quad (105), \\ A_2[VI(c)]^{(e,m)} &= \Delta M_{8LLEp}^{(e,m)} + \Delta M_{8LLFp}^{(e,m)} + \Delta M_{8LLGp}^{(e,m)} + \Delta M_{8LLHp}^{(e,m)} + \Delta M_{8LLIp}^{(e,m)} - 2\Delta B_2 M_{6LLp}^{(e,m)} \\ &= -5.2514 \quad (129), \\ A_2[VI(c)] &= A_2[VI(c)]^{(e,e)} + A_2[VI(c)]^{(m,e)} + A_2[VI(c)]^{(e,m)} \\ &= -36.5763 \quad (1141), \end{aligned} \quad (52)$$



$$\begin{aligned}
A_2[VI(e)]^{(e,e)} &= \Delta M_{8LLEq}^{(e,e)} + \Delta M_{8LLFq}^{(e,e)} + \Delta M_{8LLGq}^{(e,e)} + \Delta M_{8LLHq}^{(e,e)} + \Delta M_{8LLIq}^{(e,e)} \\
&\quad - 2\Delta B_{2,p^2}^{(m,e)} M_{6LL} \\
&= 0.7524 \quad (1338), \\
A_2[VI(e)]^{(m,e)} &= \Delta M_{8LLEq}^{(m,e)} + \Delta M_{8LLFq}^{(m,e)} + \Delta M_{8LLGq}^{(m,e)} + \Delta M_{8LLHq}^{(m,e)} + \Delta M_{8LLIq}^{(m,e)} \\
&\quad - 2\Delta B_{2,p^2}^{(m,e)} M_{6LL}^{(m,m)} \\
&= -3.9789 \quad (78), \\
A_2[VI(e)]^{(e,m)} &= \Delta M_{8LLEq}^{(e,m)} + \Delta M_{8LLFq}^{(e,m)} + \Delta M_{8LLGq}^{(e,m)} + \Delta M_{8LLHq}^{(e,m)} + \Delta M_{8LLIq}^{(e,m)} \\
&\quad - 2\Delta B_{2,p^2}^{(m,m)} M_{6LL} \\
&= -1.0950 \quad (35), \\
A_2[VI(e)] &= A_2[VI(e)]^{(e,e)} + A_2[VI(e)]^{(m,e)} + A_2[VI(e)]^{(e,m)} \\
&= -4.3215 \quad (1341), \tag{53}
\end{aligned}$$

$$\begin{aligned}
A_2[VI(f)]^{(e,e)} &= \Delta M_{8LLAp}^{(e,e)} + \Delta M_{8LLBp}^{(e,e)} + \Delta M_{8LLCp}^{(e,e)} + \Delta M_{8LLDp}^{(e,e)} - 3\Delta B_2 M_{6LLp}^{(e,e)} \\
&= -45.0425 \quad (1463), \\
A_2[VI(f)]^{(m,e)} &= \Delta M_{8LLAp}^{(m,e)} + \Delta M_{8LLBp}^{(m,e)} + \Delta M_{8LLCp}^{(m,e)} + \Delta M_{8LLDp}^{(m,e)} - 3\Delta B_2 M_{6LLp}^{(m,e)} \\
&= 8.7673 \quad (228), \\
A_2[VI(f)]^{(e,m)} &= \Delta M_{8LLAp}^{(e,m)} + \Delta M_{8LLBp}^{(e,m)} + \Delta M_{8LLCp}^{(e,m)} + \Delta M_{8LLDp}^{(e,m)} - 3\Delta B_2 M_{6LLp}^{(e,m)} \\
&= -1.8847 \quad (155), \\
A_2[VI(f)] &= A_2[VI(f)]^{(e,e)} + A_2[VI(f)]^{(m,e)} + A_2[VI(f)]^{(e,m)} \\
&= -38.1598 \quad (1488), \tag{54}
\end{aligned}$$

$$\begin{aligned}
A_2[VI(i)]^{(e,e)} &= \Delta M_{8LLAq}^{(e,e)} + \Delta M_{8LLBq}^{(e,e)} + \Delta M_{8LLCq}^{(e,e)} + \Delta M_{8LLDq}^{(e,e)} - 3\Delta B_{2,p^2}^{(e,e)} M_{6LL} \\
&= -28.3367 \quad (1142), \\
A_2[VI(i)]^{(m,e)} &= \Delta M_{8LLAq}^{(m,e)} + \Delta M_{8LLBq}^{(m,e)} + \Delta M_{8LLCq}^{(m,e)} + \Delta M_{8LLDq}^{(m,e)} - 3\Delta B_{2,p^2}^{(m,e)} M_{6LL}^{(m,m)} \\
&= 2.0977 \quad (105), \\
A_2[VI(i)]^{(e,m)} &= \Delta M_{8LLAq}^{(e,m)} + \Delta M_{8LLBq}^{(e,m)} + \Delta M_{8LLCq}^{(e,m)} + \Delta M_{8LLDq}^{(e,m)} - 3\Delta B_{2,p^2}^{(e,m)} M_{6LL} \\
&= -1.0983 \quad (31), \\
A_2[VI(i)] &= A_2[VI(i)]^{(e,e)} + A_2[VI(i)]^{(m,e)} + A_2[VI(i)]^{(e,m)} \\
&= -27.3373 \quad (1147). \tag{55}
\end{aligned}$$

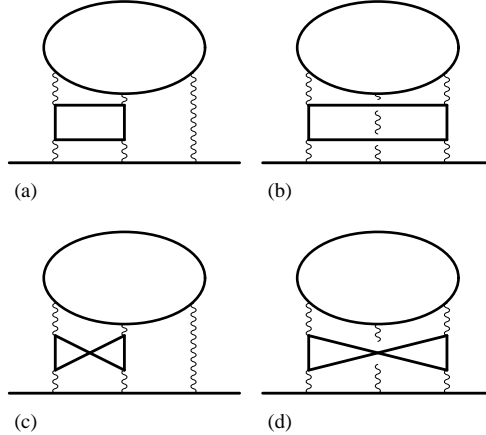


FIG. 7: Subset VI[j]

The last columns of Table X and Table XII show that the factor  $r$  is roughly equal to  $3K_\eta$  with  $K_\eta \simeq 2$  for sets VI(c) and VI(f). These factors vary from diagram to diagram within each set, making naive estimates for the sums of diagrams given in (27) entirely different from the corresponding terms of (52) - (55) obtained by explicit numerical integration. The "enhancement" factor is  $K_\eta \sim 1$  for sets VI(e) and VI(i). Table XI and Table XIII show that  $K_\eta \sim 1$  in these cases, indicating that there is no significant enhancement. This is probably because  $\Pi_2$  is buried deep in other subdiagrams in these cases.

Among the remaining subsets the subset VI(k) is likely to be the largest and most challenging because it has a subdiagram  $\Lambda_6$  which consists of 120 proper lepton loops to which six photon lines are attached. See Fig. 8. This is a diagram which appears for the first time in the tenth-order so that it cannot be derived from or related to lower-order diagrams.

Another point of interest is that its leading logarithmic term is known (29) and was used to estimate its contribution to  $a_\mu^{(10)}$ . However, to determine the actual contribution of VI(k) we must find the nonleading term, too. To answer this question it is best to evaluate VI(k) explicitly.

It turned out that this is not difficult. Our first step is to reduce the number of independent integrals to 12 using the Ward-Takahashi identity, and reduce it further to 9 using the time-reversal symmetry[51]. Each integral generated by FORM has more than 90,000 terms occupying about 30,000 lines of FORTRAN code. This is certainly huge, but not unmanageable since it is only 30 times larger than typical eighth-order integrals. We also note that this subset is particularly simple in the sense that it is entirely free from UV- and

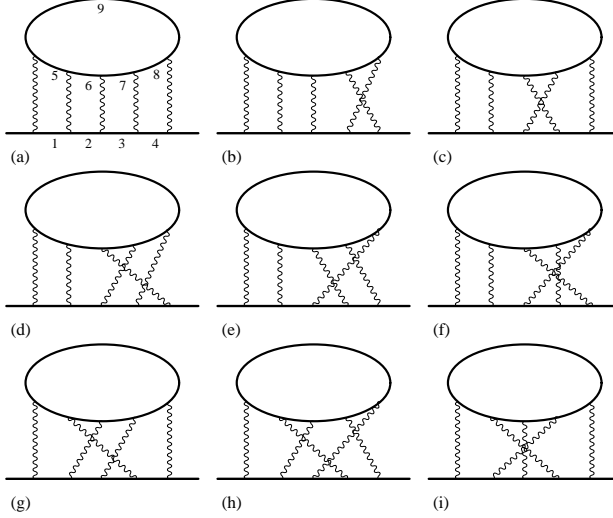


FIG. 8: Subset VI[k]

IR-divergences. Numerical integration over 13-dimensional Feynman parameter space can be handled without difficulty by VEGAS. The result of numerical integration is listed in Table XV, from which we obtain

$$A_2[VI(k)] = 97.123 \quad (62).$$

Clearly the previous estimate was an overestimate by about 100.

Another possibly large term is VI(j) [162 vertex diagrams] which we decided to evaluate explicitly. See Fig. 7. With the help of Ward-Takahashi identity and time-reversal invariance it can be represented by four independent integrals. FORM generated about 42,000 terms for each integral occupying about 18,000 lines of FORTRAN code. The result of numerical integration is listed in Table XIV, from which we obtain

$$A_2[VI(j)] = -25.505 \quad (57).$$

The subsets yet to be evaluated are VI(d), VI(g), and VI(h). We foresee no technical problem in dealing with these subsets.

Some results described in this section can be compared with the results obtained by the renormalization group method. See [50] for details.

## VI. CONTRIBUTION TO ELECTRON G-2

All Tables also contain values of mass-independent contributions from 958 vertex diagrams belonging to 17 gauge-invariant subsets. These are actually contributions to  $A_1^{(10)}$ , namely the electron g-2. Their values, including residual renormalization terms whenever they are required, are listed below:

$$\begin{aligned}
A_1[I(a)] &= 4.7094 (6) \times 10^{-4}, \\
A_1[I(b)] &= 7.0108 (7) \times 10^{-3}, \\
A_1[I(c)] &= 2.3468 (2) \times 10^{-2}, \\
A_1[I(d)] &= 4.4517 (5) \times 10^{-3}, \\
A_1[I(e)] &= 1.0296 (4) \times 10^{-2}, \\
A_1[I(f)] &= 8.4459 (14) \times 10^{-3}.
\end{aligned} \tag{58}$$

$$\begin{aligned}
A_1[II(a)] &= 4.130 (90) \times 10^{-3}, \\
A_1[II(b)] &= -5.422 (4) \times 10^{-2}, \\
A_1[II(f)] &= -2.434 (2).
\end{aligned} \tag{59}$$

$$\begin{aligned}
A_1[VI(a)] &= 1.0417 (4), \\
A_1[VI(b)] &= 1.3473 (3), \\
A_1[VI(c)] &= -2.5922 (34), \\
A_1[VI(e)] &= -0.4312 (6), \\
A_1[VI(f)] &= 0.7703 (24), \\
A_1[VI(i)] &= -0.0438 (11), \\
A_1[VI(j)] &= -0.2288 (17), \\
A_1[VI(k)] &= 0.6802 (38).
\end{aligned} \tag{60}$$

## VII. DISCUSSION

Let us first add up all terms contributing to  $A_2^{(10)}(m_\mu/m_e)$  of muon g-2 evaluated by numerical integration. From (34), (35), (39), (38), (41), (44), (47), (49), (50), (51), (52),

(53), (54), (55), (56), (57), which represent the contributions of 2958 Feynman diagrams belonging to 17 gauge-invariant sets, we obtain

$$A_2^{(10)}(m_\mu/m_e)[\textit{partial sum}] = 662.50 \quad (27). \quad (61)$$

The uncertainties from these diagrams, which include all dominant sources of uncertainties considered previously, have been reduced to an insignificant level. Note, however, that some terms which were not included in previous estimates turned out to be not negligible.

Of course, the real value of  $A_2^{(10)}(m_\mu/m_e)$  is not known until remaining diagrams are evaluated. However, they have no known mechanism for giving rise to large values and likely to remain modest in size and uncertainty. We therefore expect that the final value will stay within the range

$$A_2^{(10)}(m_\mu/m_e)[\textit{estimate}] = 663 \quad (20). \quad (62)$$

This will reduce (16) by  $1.81 \times 10^{-11}$ .

Our next step is to evaluate 6122 vertex diagrams from the remaining 14 gauge-invariant subsets. Many of these diagrams can be integrated by means of available information on  $\Pi$  and  $\Lambda$ . They include:

1. Subsets I(f), I(g), I(h) of Set I.
2. Subsets II(c), II(d) of Set II.
3. Subsets III(a) and III(b) of Set III.
4. All diagrams of Set IV, which can be evaluated by simple modification of codes of Group V of eighth-order diagrams.

These subsets are on our next time schedule.

The remainder of diagrams are more difficult to evaluate for the following reasons:

1. Subsets I(i) and I(j) require the knowledge of the eighth-order v-p spectral function  $\Pi_8$  which have not yet been constructed.
2. Diagrams of set II(e) require construction of radiatively-corrected light-by-light scattering subdiagrams, which are not yet available.

3. Subset III[c] contains  $\Lambda_4$  internally.
4. Subsets VI(d), VI(g), and VI(h) have no lower-order structure upon which they can be built.

We foresee no intractable barrier for their evaluation.

As far as the electron  $g-2$  is concerned what is most important is the Set V which have no lower-order fermion loop structure. The integrands of this set are gigantic and require an enormous number of UV and IR subtraction terms. Our experience with the subsets VI(k) and VI(j) indicates, however, that their sizes are still manageable with available computers. What is really crucial for their evaluation, however, is that all steps of construction of integrand must be fully automated. Thus far we have succeeded in obtaining a code that handles renormalization of ultraviolet divergence automatically [49]. For the moment the infrared divergence is treated by giving a small cutoff mass  $\lambda$  to the photon. A code for cutoff-independent treatment of IR divergence is being developed.

### Acknowledgments

T. K.'s work is supported by the U. S. National Science Foundation under Grant No. PHY-0098631. T. K. thanks the Eminent Scientist Invitation Program of RIKEN, Japan, for the hospitality extended to him where a part of this work was carried out. T. K. is also supported during his stay in Japan by Ministry of Education, Science and Culture of Japan, Grant-in-Aid for Scientific Research on Priority Areas, 13134101.

M. N.'s work is partly supported by Japan Society for the Promotion of Science, Grant-in-Aid for Scientific Research (C) 15540303, 2003-2005.

The numerical work has been carried out on the RIKEN Super Combined Cluster System (RSCC).

- 
- [1] P. Kusch and H. M. Foley, Phys. Rev. **72**, 1256 (1947).
  - [2] J. Schwinger, Phys. Rev. **73**, 416L (1948).
  - [3] W. E. Lamb, Sr., and R. C. Retherford, Phys. Rev. **72**, 241 (1947).
  - [4] A. Rich and J. C. Wesley, Rev. Mod. Phys. **44**, 250 (1972).

- [5] R. S. Van Dyck, Jr., P. B. Schwinberg and H. G. Dehmelt, Phys. Rev. Lett. **59**, 26 (1987).
- [6] R. S. Van Dyck, Jr., et al., 1991, unpublished.
- [7] R. Mittleman, H. Dehmelt and S. Kim, Phys. Rev. Lett. **75**, 2839 (1995).
- [8] L. S. Brown, G. Gabrielse, K. Helmerson, and J. Tan, Phys. Rev. Lett. **55**, 44 (1985).
- [9] B. Odom, Ph. D. thesis, Harvard University, 2005.
- [10] A. Petermann, Helv. Phys. Acta **30**, 407 (1957).
- [11] C. Sommerfeld, Phys. Rev. **107**, 328 (1957).
- [12] T. Kinoshita, Phys. Rev. Lett. **75**, 4728 (1995).
- [13] S. Laporta and E. Remiddi, Phys. Lett. B **379**, 283 (1996).
- [14] T. Kinoshita and M. Nio, Phys. Rev. D **73**, 013003 (2006).
- [15] V. W. Hughes and T. Kinoshita, Rev. Mod. Phys. **71**, S133 (1999).
- [16] F. Jegerlehner, private communication, 1996.
- [17] B. Krause, private communication, 1996.
- [18] A. Czarnecki, B. Krause, and W. J. Marciano, Phys. Rev. Lett. **76**, 3267 (1996).
- [19] A. Wicht *et al.*, Physica Scripta T**102**, 82 (2002).
- [20] P. J. Mohr and B. N. Taylor, Rev. Mod. Phys. **77**, 1 (2005).
- [21] J. Bailey *et al.*, Phys. Lett. **68B**, 191 (1977); F. J. M. Farley and E. Picasso, in *Quantum Electrodynamics*, edited by T. Kinoshita (World Scientific, Singapore, 1990), pp. 479 - 559.
- [22] G. W. Bennett *et al.*, Phys. Rev. Lett. **92**, 161802 (2004).
- [23] G. W. Bennett *et al.*, Phys. Rev. Lett. **89**, 101804 (2002).
- [24] H. N. Brown *et al.*, Phys. Rev. Lett. **86**, 2227 (2001).
- [25] H. N. Brown *et al.*, Phys. Rev. D **62**, 091101 (2000).
- [26] A. Czarnecki and W. J. Marciano, Phys. Rev. D **64**, 013014 (2001).
- [27] M. Davier and A. Höcker, Phys. Lett. **B435**, 427 (1998).
- [28] S. Narison, Phys. Lett. **B513**, 53 (2001).
- [29] J. F. de Troconiz and F. J. Yndurain, Phys. Rev. D **65**, 093001 (2002).
- [30] M. Knecht and A. Nyffeler, Phys. Rev. D **65**, 073034 (2002); M. Knecht, A. Nyffeler, M. Perrottet, and E. de Rafael, Phys. Rev. Lett. **88**, 071802 (2002); M. Hayakawa and T. Kinoshita (2001), hep-ph/0112102; J. Bijnens, E. Pallante, and J. Prades, Nucl. Phys. **B626**, 410 (2002); I. Blokland, A. Czarnecki, and K. Melnikov, Phys. Rev. Lett. **88**, 071803 (2002).
- [31] M. J. Ramsey-Musolf and M. B. Wise, Phys. Rev. Lett. **89**, 041601 (2002).

- [32] A. Höcker, hep-ph/0410081 (2004).
- [33] K. Hagiwara, A. D. Martin, D. Nomura, T. Teubner, Phys. Rev. D **69**, 093003 (2004).
- [34] J. F. de Troconiz and F. J. Yndurain, Phys. Rev. D **71**, 073008 (2005).
- [35] K. Melnikov and A. Vainshtein, Phys. Rev. D **70**, 113006 (2004).
- [36] M. Knecht et al., JHEP **11**. 003 (2002).
- [37] A. Czarnecki, W. J. Marciano, and A. Vainshtein, Phys. Rev.D **67**, 073006 (2003).
- [38] T. Kinoshita and M. Nio, Phys. Rev. Lett. **90**, 021803 (2003).
- [39] T. Kinoshita and M. Nio, Phys. Rev. D **70**, 113001 (2005).
- [40] T. Kinoshita, Nucl. Phys. B (Proc. Suppl.) **144**, 206 (2005).
- [41] S. Laporta, Phys. Lett. B **328**, 522 (1994).
- [42] T. Kinoshita and W. J. Marciano, in *Quantum Electrodynamics*, edited by T. Kinoshita (World Scientific, Singapore, 1990), pp. 419 - 478.
- [43] S. G. Karshenboim, Yad. Fiz. **56**, 252 (1993) [Phys. At. Nucl. **56**, 857 (1993)].
- [44] A. S. Elikhovskii, Yad. Fiz. **49**, 1056 (1989) [Sov. J. Phys. **49**, 654 (1989)].
- [45] A. L. Kataev, Phys. Lett. B **284**, 401 (1992).
- [46] S. Laporta and E. Remiddi, Phys. Lett. B **301**, 440 (1993).
- [47] T. Kaneko, Comp. Phys. Comm. **92**, 127 (1995).
- [48] A. I. Milstein and A. S. Yelkhovsky, Phys. Lett. **233B**, 11 (1989).
- [49] T. Aoyama, M. Hayakawa, T. Kinoshita, and M. Nio, hep-ph/0512288.
- [50] A. L. Kataev, hep-ph/0507174.
- [51] We noticed that  $X6k_f$  is actually identical with  $X6k_b$  while checking the proof. Thus the number of independent integrals of set VI is 8, not 9. Fortunately this does not affect our numerical result given in Eq. (56).



TABLE I: Numerical evaluation of diagrams of subsets (a), (b), (c), and (e) of Set I. The notation follows that of [42] with some modification and adaptation.  $n_F$  is the number of Feynman diagrams represented by the integral.

Integral	$n_F$	Value (error) including $n_F$	Sampling per iteration	No. of iterations
$M_{2,p2:4}^{(e,e,e,e)}$	1	20.14293 (23)	$1 \times 10^8$	180
$M_{2,p2:4}^{(e,e,e,m)}$	4	2.20327 ( 9)	$1 \times 10^7$	80
$M_{2,p2:4}^{(e,e,m,m)}$	6	0.20697 ( 2)	$1 \times 10^7$	20
$M_{2,p2:4}^{(e,m,m,m)}$	4	0.01388 ( 1)	$1 \times 10^7$	20
$M_{2,p2:4}^{(m,m,m,m)}$	1	$4.7094 (6) \times 10^{-4}$	$1 \times 10^7$	20
$M_{2,p4,p2:2}^{(e,e,e)}$	9	27.69038 (30)	$4 \times 10^8$	190
$M_{2,p4,p2:2}^{(e,m,e)}$	18	1.16628 ( 9)	$1 \times 10^7$	100
$M_{2,p4,p2:2}^{(e,m,m)}$	9	0.03182 ( 3)	$1 \times 10^6$	20
$M_{2,p4,p2:2}^{(m,e,e)}$	9	1.61436 ( 6)	$1 \times 10^7$	120
$M_{2,p4,p2:2}^{(m,m,e)}$	18	0.16470 ( 5)	$1 \times 10^6$	20
$M_{2,p4,p2:2}^{(m,m,m)}$	9	$7.0108 (7) \times 10^{-3}$	$1 \times 10^7$	20
$M_{2,p4:2}^{(e,e)}$	9	4.74212 (14)	$1 \times 10^8$	220
$M_{2,p4:2}^{(e,m)}$	18	0.39926 ( 3)	$1 \times 10^7$	120
$M_{2,p4:2}^{(m,m)}$	9	$2.3468 (2) \times 10^{-2}$	$1 \times 10^7$	20
$M_{2,p6p2}^{(e,e)}$	30	- 1.20841 (70)	$1 \times 10^8$	100
$M_{2,p6p2}^{(e,m)}$	30	- 0.02110 ( 4)	$1 \times 10^7$	120
$M_{2,p6p2}^{(m,e)}$	30	0.01031 ( 1)	$1 \times 10^6$	20
$M_{2,p6p2}^{(m,m)}$	30	$1.0296 (4) \times 10^{-2}$	$1 \times 10^7$	20

TABLE II: Numerical evaluation of diagrams of subsets (d) of Set I. The notation follows that of [42] with some modification and adaptation.  $n_F$  is the number of Feynman diagrams represented by the integral. Subscripts  $p4A$ ,  $p4B$  refer to part of fourth-order  $v - p$   $\Pi_4$  containing vertex correction and self-energy insertion, respectively. The last four lines are values obtained using the exact sixth-order spectral function  $\Pi_{4(2)}$ .

Integral	$n_F$	Value (error) including $n_F$	Sampling per iteration	No. of iterations
$M_{2,p4A(p2)p2}^{(e(e),e)}$	2	2.63064 (72)	$1 \times 10^7$	80
$M_{2,p4A(p2)p2}^{(m(e),e)}$	2	0.76997 ( 7)	$1 \times 10^7$	40
$M_{2,p4A(p2)p2}^{(e(m),e)}$	2	0.12703 ( 2)	$1 \times 10^7$	40
$M_{2,p4A(p2)p2}^{(m(m),e)}$	2	$7.3352 ( 7) \times 10^{-2}$	$1 \times 10^7$	40
$M_{2,p4A(p2)p2}^{(e(e),m)}$	2	$1.3211 (18) \times 10^{-2}$	$1 \times 10^7$	79
$M_{2,p4A(p2)p2}^{(m(e),m)}$	2	$3.5428 ( 4) \times 10^{-2}$	$1 \times 10^7$	40
$M_{2,p4A(p2)p2}^{(e(m),m)}$	2	$5.0276 ( 6) \times 10^{-3}$	$1 \times 10^7$	40
$M_{2,p4A(p2)p2}^{(m(m),m)}$	2	$3.8330 ( 4) \times 10^{-3}$	$1 \times 10^7$	40
$M_{2,p4B(p2)p2}^{(e(e),e)}$	4	5.51053 (70)	$1 \times 10^7$	80
$M_{2,p4B(p2)p2}^{(m(e),e)}$	4	0.63490 ( 9)	$1 \times 10^7$	40
$M_{2,p4B(p2)p2}^{(e(m),e)}$	4	$3.9114 (47) \times 10^{-3}$	$1 \times 10^7$	29
$M_{2,p4B(p2)p2}^{(m(m),e)}$	4	$1.1129 ( 4) \times 10^{-2}$	$1 \times 10^7$	29
$M_{2,p4B(p2)p2}^{(e(e),m)}$	4	0.15798 ( 2)	$1 \times 10^7$	80
$M_{2,p4B(p2)p2}^{(m(e),m)}$	4	$3.2133 ( 5) \times 10^{-2}$	$1 \times 10^7$	40
$M_{2,p4B(p2)p2}^{(e(m),m)}$	4	$2.6449 (19) \times 10^{-4}$	$1 \times 10^7$	40
$M_{2,p4B(p2)p2}^{(m(m),m)}$	4	$6.1873 (17) \times 10^{-4}$	$1 \times 10^7$	40
$M_{2,p4(p2)p2}^{(e(e),e)}$	6	7.45270 (88)	$1 \times 10^8$	140
$M_{2,p4(p2)p2}^{(e(e),m)}$	6	0.15853 (10)	$1 \times 10^7$	120
$M_{2,p4(p2)p2}^{(m(m),e)}$	6	0.07173 ( 3)	$1 \times 10^6$	20
$M_{2,p4(p2)p2}^{(m(m),m)}$	6	$3.8028 (5) \times 10^{-3}$	$1 \times 10^7$	20

TABLE III: Numerical evaluation of diagrams of subsets (f) of Set I. The notation follows that of [42] with some modification and adaptation.  $n_F$  is the number of Feynman diagrams represented by the integral. Subscripts  $p4A$ ,  $p4B$  refer to part of fourth-order  $v - p$   $\Pi_4$  containing vertex correction and self-energy insertion, respectively.

Integral	$n_F$	Value (error) including $n_F$	Sampling per iteration	No. of iterations
$\Delta M_{2,p4A(p2:2)}^{(e(e,e))}$	1	1.99747 (10)	$4 \times 10^7$	240
$\Delta M_{2,p4A(p2:2)}^{(e(e,m))}$	2	0.15863 (3)	$1 \times 10^7$	20
$\Delta M_{2,p4A(p2:2)}^{(e(m,m))}$	1	$1.0612 (2) \times 10^{-2}$	$1 \times 10^7$	20
$\Delta M_{2,p4A(p2:2)}^{(m(e,e))}$	1	0.44361 (6)	$1 \times 10^7$	20
$\Delta M_{2,p4A(p2:2)}^{(m(e,m))}$	2	$9.4542 (13) \times 10^{-2}$	$1 \times 10^7$	20
$\Delta M_{2,p4A(p2:2)}^{(m(m,m))}$	1	$8.1763 (13) \times 10^{-3}$	$1 \times 10^7$	20
$\Delta M_{2,p4B(p2:2)}^{(e(e,e))}$	2	0.94959 (11)	$1 \times 10^7$	340
$\Delta M_{2,p4B(p2:2)}^{(e(e,m))}$	4	$2.5573 (56) \times 10^{-3}$	$1 \times 10^7$	20
$\Delta M_{2,p4B(p2:2)}^{(e(m,m))}$	2	$1.6448 (275) \times 10^{-5}$	$1 \times 10^7$	20
$\Delta M_{2,p4B(p2:2)}^{(m(e,e))}$	2	0.26023 (6)	$1 \times 10^7$	20
$\Delta M_{2,p4B(p2:2)}^{(m(e,m))}$	4	$1.1060 (5) \times 10^{-2}$	$1 \times 10^7$	20
$\Delta M_{2,p4B(p2:2)}^{(m(m,m))}$	2	$2.6957 (32) \times 10^{-4}$	$1 \times 10^7$	20

TABLE IV: Numerical evaluation of set II(a) which consists of II( $a_1$ ) and II( $a_2$ ). The set II( $a_1$ ) has contributions denoted by  $\Delta_1$  and set II( $a_2$ ) has contributions denoted by  $\Delta_2$ . The symbol  $()()$  indicates photon lines in which v-p loops  $\Pi$  are inserted.  $n_F$  is the number of Feynman diagrams represented by the integral. t.r. is time-reversed Feynman diagram.

Integral	$n_F$	Value (error) including $n_F$	Sampling per iteration	No. of iterations
$\Delta_1 M_{4a,p2:3}^{(e,e,e)()} + \text{t.r.}$	6	15.15611 (283)	$1 \times 10^8$	160
$\Delta_1 M_{4a,p2:3}^{(e,e,m)()} + \text{t.r.}$	18	1.31796 ( 49)	$1 \times 10^8$	200
$\Delta_1 M_{4a,p2:3}^{(e,m,m)()} + \text{t.r.}$	18	0.09109 ( 13)	$1 \times 10^8$	100
$\Delta_1 M_{4a,p2:3}^{(m,m,m)()} + \text{t.r.}$	6	0.00413 ( 9)	$1 \times 10^7$	20
$\Delta_1 M_{4b,p2:3}^{(e,e,e)()} + \Delta_1 M_{4b,p2:3}^{(){}(e,e,e)}$	6	-30.09130 (191)	$4 \times 10^7$	200
$\Delta_1 M_{4b,p2:3}^{(e,e,m)()} + \Delta_1 M_{4b,p2:3}^{(){}(e,e,m)}$	18	-6.38188 ( 26)	$1 \times 10^8$	100
$\Delta_1 M_{4b,p2:3}^{(e,m,m)()} + \Delta_1 M_{4b,p2:3}^{(){}(e,m,m)}$	18	-0.84226 ( 4)	$1 \times 10^8$	120
$\Delta_1 M_{4b,p2:3}^{(m,m,m)()} + \Delta_1 M_{4b,p2:3}^{(){}(m,m,m)}$	6	-0.05422 ( 4)	$1 \times 10^7$	20
$\Delta_2 M_{4a,p2:2,p2}^{(e,e)(e)} + \text{t.r.}$	6	12.23457 (99)	$2 \times 10^8$	370
$\Delta_2 M_{4a,p2:2,p2}^{(e,e)(m)} + \text{t.r.}$	6	0.01971 (34)	$1 \times 10^7$	120
$\Delta_2 M_{4a,p2:2,p2}^{(e,m)(e)} + \text{t.r.}$	12	0.27276(35)	$2 \times 10^7$	380
$\Delta_2 M_{4a,p2:2,p2}^{(m,m)(e)} + \text{t.r.}$	6	-0.01408(27)	$1 \times 10^7$	20
$\Delta_2 M_{4a,p2:2,p2}^{(e,m)(m)} + \text{t.r.}$	12	-0.08222(22)	$1 \times 10^7$	20
$\Delta_2 M_{4a,p2:2,p2}^{(m,m)(m)} + \text{t.r.}$	6	-0.00998( 3)	$1 \times 10^7$	20
$\Delta_2 M_{4b,p2:2,p2}^{(e,e)(e)} + \Delta_2 M_{4b,p2,p2:2}^{(e)(e,e)}$	6	-28.69942 ( 79)	$1 \times 10^8$	380
$\Delta_2 M_{4b,p2:2,p2}^{(e,e)(m)} + \Delta_2 M_{4b,p2,p2:2}^{(m)(e,e)}$	6	-1.72076 (14)	$1 \times 10^7$	100
$\Delta_2 M_{4b,p2:2,p2}^{(e,m)(e)} + \Delta_2 M_{4b,p2,p2:2}^{(e)(e,m)}$	12	-3.71561 (32)	$1 \times 10^7$	120
$\Delta_2 M_{4b,p2:2,p2}^{(m,m)(e)} + \Delta_2 M_{4b,p2,p2:2}^{(e)(m,m)}$	6	-0.23956 ( 8)	$1 \times 10^7$	20
$\Delta_2 M_{4b,p2:2,p2}^{(e,m)(m)} + \Delta_2 M_{4b,p2,p2:2}^{(m)(e,m)}$	12	-0.37976 ( 7)	$1 \times 10^7$	20
$\Delta_2 M_{4b,p2:2,p2}^{(m,m)(m)} + \Delta_2 M_{4b,p2,p2:2}^{(m)(m,m)}$	6	-0.03619 ( 1)	$1 \times 10^7$	20

TABLE V: Numerical evaluation of diagrams of set II(b).  $\Delta_1$  indicates contributions in which  $\Pi$ 's act on the same photon line while  $\Delta_2$  refers to those in which  $\Pi$ 's act on different photon lines. The symbol  $()()$  indicates photon lines in which v-p loops  $\Pi$  are inserted.  $n_F$  is the number of Feynman diagrams represented by the integral. t.r. is time-reversed Feynman diagram.

Integral	$n_F$	Value (error) including $n_F$	Sampling per iteration	No. of iterations
$\Delta_1 M_{4a,p4p2}^{(e,e)()} + (p4 \leftrightarrow p2) + \text{t.r.}$	36	12.65000 (135)	$4 \times 10^8$	220
$\Delta_1 M_{4a,p4p2}^{(e,m)()} + (p4 \leftrightarrow p2) + \text{t.r.}$	36	0.30749 ( 22)	$4 \times 10^7$	140
$\Delta_1 M_{4a,p4p2}^{(m,e)()} + (p4 \leftrightarrow p2) + \text{t.r.}$	36	0.84809 ( 23)	$1 \times 10^8$	160
$\Delta_1 M_{4a,p4p2}^{(m,m)()} + (p4 \leftrightarrow p2) + \text{t.r.}$	36	0.04424 ( 33)	$1 \times 10^7$	20
$\Delta_1 M_{4b,p4p2}^{(e,e)()} + \Delta_1 M_{4b,p4p2}^{()^{(e,e)}} + (p4 \leftrightarrow p2)$	36	-19.70781 (143)	$1 \times 10^8$	220
$\Delta_1 M_{4b,p4p2}^{(e,m)()} + \Delta_1 M_{4b,p4p2}^{()^{(e,m)}} + (p4 \leftrightarrow p2)$	36	-1.23984 ( 10)	$4 \times 10^7$	140
$\Delta_1 M_{4b,p4p2}^{(m,e)()} + \Delta_1 M_{4b,p4p2}^{()^{(m,e)}} + (p4 \leftrightarrow p2)$	36	-3.06974 ( 9)	$1 \times 10^8$	200
$\Delta_1 M_{4b,p4p2}^{(m,m)()} + \Delta_1 M_{4b,p4p2}^{()^{(m,m)}} + (p4 \leftrightarrow p2)$	36	-0.30984 ( 15)	$1 \times 10^7$	20
$\Delta_2 M_{4a,p4p2}^{(e)(e)} + \text{t.r.}$	18	5.89471 (107)	$1 \times 10^8$	240
$\Delta_2 M_{4a,p4p2}^{(e)(m)} + \text{t.r.}$	18	0.09286 ( 16)	$1 \times 10^7$	140
$\Delta_2 M_{4a,p4p2}^{(m)(e)} + \text{t.r.}$	18	0.21886 ( 23)	$1 \times 10^7$	180
$\Delta_2 M_{4a,p4p2}^{(m)(m)} + \text{t.r.}$	18	-0.01723 ( 5)	$1 \times 10^7$	20
$\Delta_2 M_{4b,p4p2}^{(e)(e)} + (p4 \leftrightarrow p2)$	18	-9.83570 (97)	$4 \times 10^7$	260
$\Delta_2 M_{4b,p4p2}^{(e)(m)} + (p4 \leftrightarrow p2)$	18	-0.56867 ( 8)	$1 \times 10^7$	120
$\Delta_2 M_{4b,p4p2}^{(m)(e)} + (p4 \leftrightarrow p2)$	18	-1.36297 (13)	$1 \times 10^7$	100
$\Delta_2 M_{4b,p4p2}^{(m)(m)} + (p4 \leftrightarrow p2)$	18	-0.10756 ( 2)	$1 \times 10^7$	20

TABLE VI: Numerical evaluation of diagrams for auxiliary quantities needed to evaluate contribution of Set I and Set II.

Integral	$n_F$	Value (error) including $n_F$	Sampling per iteration	No. of iterations
$\Delta B_{2,2:3}^{(e,e,e)}$	1	16.15765 (75)	$1 \times 10^7$	100
$\Delta B_{2,2:3}^{(e,e,m)}$	3	2.71594 (12)	$1 \times 10^7$	100
$\Delta B_{2,2:3}^{(e,m,m)}$	3	0.36136 ( 4)	$1 \times 10^7$	40
$\Delta B_{2,2:3}^{(m,m,m)}$	1	0.02381 ( 1)	$1 \times 10^7$	20
$\Delta B_{2,p4p2}^{(e,e)}$	6	13.27621 (93)	$1 \times 10^7$	100
$\Delta B_{2,p4p2}^{(e,m)}$	6	0.53279 ( 5)	$1 \times 10^7$	80
$\Delta B_{2,p4p2}^{(m,e)}$	6	1.31884 ( 5)	$1 \times 10^7$	120
$\Delta B_{2,p4p2}^{(m,m)}$	6	0.13066 ( 2)	$1 \times 10^7$	20
$\Delta B_{2,p2:2}^{(e(e,e))}$	1	0.02791 ( 1)	$1 \times 10^6$	40
$\Delta B_{2,p2:2}^{(m(e,e))}$	1	5.33035 (20)	$1 \times 10^7$	100
$\Delta B_{2,p2:2}^{(m(m,e))}$	2	0.47208 ( 9)	$1 \times 10^6$	40
$\Delta B_{2,p2:2}^{(e(m,e))}$	2	$3.6159 (8) \times 10^{-5}$	$1 \times 10^6$	40
$\Delta B_{2,p2:2}^{(e(m,m))}$	1	$8.3020 (36) \times 10^{-7}$	$1 \times 10^6$	20

TABLE VII: Numerical evaluation of diagrams of set II(f) in Version A. The suffix  $p$  indicates insertion of  $\Pi_2$  in the photon lines connecting the muon line and the  $l-l$  loop.  $A_2[2f]^{(x,y)} \equiv \Delta M_{8LLJp}^{(x,y)} + \Delta M_{8LLKp}^{(x,y)} + \Delta M_{8LLLp}^{(x,y)}$ .  $r = \Delta M_{8LLxp} / \Delta M_{8LLx}$ , where  $x = J, K, L$ , in column 6 is for comparison with the enhancement factor  $4K_\eta$  for set II(f) discussed in Sec. III. The logarithmic enhancement comes from the  $v-p$  loop only. This is consistent with  $r \simeq 11 \sim 15$  for (e,e), (me) and  $r \simeq 0.7 \sim 2$  for (e,m), (m,m).

Integral	$n_F$	Value (error) including $n_F$	Sampling per iteration	No. of iterations	$r$
$\Delta M_{8LLJp}^{(e,e)}$	24	70.6567 (254)	$4 \times 10^7$	220	11.05
$\Delta M_{8LLJp}^{(m,e)}$	24	35.0760 ( 78)	$2 \times 10^7$	200	13.74
$\Delta M_{8LLJp}^{(e,m)}$	24	6.0056 ( 26)	$2 \times 10^7$	200	0.94
$\Delta M_{8LLJp}^{(m,m)}$	24	3.7717 ( 17)	$1 \times 10^7$	140	1.48
$\Delta M_{8LLKp}^{(e,e)}$	24	-87.8367 (291)	$8 \times 10^7$	210	11.29
$\Delta M_{8LLKp}^{(m,e)}$	24	-26.1793 ( 83)	$2 \times 10^7$	220	13.97
$\Delta M_{8LLKp}^{(e,m)}$	24	-5.4760 ( 29)	$2 \times 10^7$	230	0.70
$\Delta M_{8LLKp}^{(m,m)}$	24	-2.9311 ( 17)	$1 \times 10^7$	140	1.56
$\Delta M_{8LLLp}^{(e,e)}$	24	-39.9514 (287)	$4 \times 10^7$	310	13.07
$\Delta M_{8LLLp}^{(m,e)}$	24	-24.5877 ( 81)	$2 \times 10^7$	220	14.73
$\Delta M_{8LLLp}^{(e,m)}$	24	-5.2468 ( 29)	$2 \times 10^7$	200	1.71
$\Delta M_{8LLLp}^{(m,m)}$	24	-3.2771 ( 17)	$1 \times 10^7$	140	1.96
$A_2[2f]^{(e,e)}$	72	-57.1314 (481)			
$A_2[2f]^{(m,e)}$	72	-15.6910 (140)			
$A_2[2f]^{(e,m)}$	72	-4.7172 ( 49)			
$A_2[2f]^{(m,m)}$	72	-2.4365 ( 29)			

TABLE VIII: Numerical evaluation of diagrams of set II(f) in Version B. The symbol  $p$  indicates insertion of  $\Pi_2$  in the photon lines connecting the muon line and the *light–light* loop.  $JKLp^{(x,y)} \equiv \Delta M_{8LLJp}^{(x,y)} + \Delta M_{8LLKp}^{(x,y)} + \Delta M_{8LLLp}^{(x,y)}$ . The suffix 2 or 13 below indicates the muon line into which the magnetic field vertex is inserted.  $A_2[2f]^{(x,y)} \equiv JKLp_2^{(x,y)} + JKLp_{13}^{(x,y)}$ .  $r = JKLp/JKL$  in column 6 is for comparison with the enhancement factor  $4K_\eta$  for set II(f) discussed in Sec. III.

Integral	$n_F$	Value (error) including $n_F$	Sampling per iteration	No. of iterations	$r$
$JKLp_2^{(e,e)}$	24	-11.37774 (313)	$1 \times 10^7, 1 \times 10^9$	250, 20	12.35
$JKLp_2^{(m,e)}$	24	-1.87116 ( 30)	$1 \times 10^7$	250	15.86
$JKLp_2^{(e,m)}$	24	-0.74946 ( 64)	$1 \times 10^7$	250	0.81
$JKLp_2^{(m,m)}$	24	-0.28035 ( 39)	$1 \times 10^7$	250	2.38
$JKLp_{13}^{(e,e)}$	48	-45.68188 (1079)	$1 \times 10^8, 1 \times 10^9$	450, 100	13.03
$JKLp_{13}^{(m,e)}$	48	-13.81420 ( 386)	$1 \times 10^7, 1 \times 10^9$	250, 40	15.82
$JKLp_{13}^{(e,m)}$	48	-3.96527 ( 399)	$1 \times 10^7$	250	1.13
$JKLp_{13}^{(m,m)}$	48	-2.15339 ( 182)	$1 \times 10^7$	250	2.47
$A_2[2f]^{(e,e)}$	72	-57.0596 (113)			
$A_2[2f]^{(m,e)}$	72	-15.6854 (39)			
$A_2[2f]^{(e,m)}$	72	-4.7147 ( 40)			
$A_2[2f]^{(m,m)}$	72	-2.4338 ( 19)			



TABLE IX: Numerical evaluation of diagrams of Set VI(a) and Set VI(b). The notation follows that of [42] with some modification and adaptation.

Integral	$n_F$	Value (error) including $n_F$	Sampling per iteration	No. of iterations
$M_{6LL,p2p2}^{(e,e,e)}$	6	542.91180 (910)	$1 \times 10^9$	300
$M_{6LL,p2p2}^{(e,e,m)}$	72	39.00349 (272)	$1 \times 10^8$	200
$M_{6LL,p2p2}^{(e,m,m)}$	36	2.43029 ( 22)	$1 \times 10^8$	200
$M_{6LL,p2p2}^{(m,e,e)}$	36	34.42389 (680)	$1 \times 10^8$	200
$M_{6LL,p2p2}^{(m,e,m)}$	72	10.37125 (162)	$1 \times 10^8$	200
$M_{6LL,p2p2}^{(m,m,m)}$	36	1.04171 ( 37)	$1 \times 10^8$	20
$M_{6LL,p4}^{(e,e)}$	54	168.72855 (478)	$1 \times 10^9$	200
$M_{6LL,p4}^{(e,m)}$	54	7.58383 ( 50)	$1 \times 10^8$	210
$M_{6LL,p4}^{(m,e)}$	54	4.81614 (164)	$1 \times 10^8$	200
$M_{6LL,p4}^{(m,m)}$	54	1.34726 ( 30)	$1 \times 10^8$	140

TABLE X: Numerical evaluation of diagrams of Set VI(c). The notation follows that of [42] with some modification and adaptation. The suffix  $p$  indicates insertion of  $\Pi_2$  in the photon lines connecting the muon line and  $l$ - $l$  loop.  $r = \Delta M_{8LLxp}/\Delta M_{8LLx}$ , where  $x = E, F, G, H, I$ , in column 6 is for comparison with the crude enhancement factor  $3K_\eta$  for set VI(c) discussed in Sec. III.

Integral	$n_F$	Value (error) including $n_F$	Sampling per iteration	No. of iterations	$r$
$\Delta M_{8LLEp}^{(e,e)}$	18	-82.9940 (141)	$2 \times 10^8$	200	3.84
$\Delta M_{8LLEp}^{(e,m)}$	18	-1.8277 ( 18)	$1 \times 10^7$	40	
$\Delta M_{8LLEp}^{(m,e)}$	18	-3.3463 ( 44)	$1 \times 10^7$	140	
$\Delta M_{8LLEp}^{(m,m)}$	18	-0.6168 ( 6)	$1 \times 10^7$	140	
$\Delta M_{8LLFp}^{(e,e)}$	36	-322.4493 ( 573)	$2 \times 10^8$	280	4.25
$\Delta M_{8LLFp}^{(e,m)}$	36	-5.2571 ( 60)	$1 \times 10^7$	80	
$\Delta M_{8LLFp}^{(m,e)}$	36	-9.3199 ( 64)	$4 \times 10^7$	390	
$\Delta M_{8LLFp}^{(m,m)}$	36	-1.5392 ( 17)	$1 \times 10^7$	280	
$\Delta M_{8LLGp}^{(e,e)}$	36	-181.5345 (489)	$2 \times 10^8$	210	5.17
$\Delta M_{8LLGp}^{(e,m)}$	36	-3.3841 ( 61)	$1 \times 10^7$	80	
$\Delta M_{8LLGp}^{(m,e)}$	36	-6.5157 ( 84)	$4 \times 10^7$	300	
$\Delta M_{8LLGp}^{(m,m)}$	36	-0.9499 ( 18)	$1 \times 10^7$	300	
$\Delta M_{8LLHp}^{(e,e)}$	18	230.3344 (590)	$4 \times 10^8$	400	4.27
$\Delta M_{8LLHp}^{(e,m)}$	18	2.2093 ( 74)	$1 \times 10^7$	66	
$\Delta M_{8LLHp}^{(m,e)}$	18	2.1519 ( 96)	$4 \times 10^7$	480	
$\Delta M_{8LLHp}^{(m,m)}$	18	0.2839 ( 18)	$1 \times 10^7$	320	
$\Delta M_{8LLIp}^{(e,e)}$	36	514.7317 (567)	$2 \times 10^8$	300	4.57
$\Delta M_{8LLIp}^{(e,m)}$	36	7.0544 ( 59)	$1 \times 10^7$	80	
$\Delta M_{8LLIp}^{(m,e)}$	36	9.2489 ( 68)	$4 \times 10^7$	320	
$\Delta M_{8LLIp}^{(m,m)}$	36	1.1912 ( 13)	$1 \times 10^7$	340	

TABLE XI: Numerical evaluation of diagrams of Set VI(e). The notation follows that of [42] with some modification and adaptation. The suffix  $q$  refers to insertion of  $\Pi_2$  in radiative corrections to the muon line.  $r = \Delta M_{8LLxp}/\Delta M_{8LLx}$ , where  $x = E, F, G, H, I$ , in column 6 is for comparison with the crude enhancement factor for set VI(e) discussed in Sec. III.

Integral	$n_F$	Value (error) including $n_F$	Sampling per iteration	No. of iterations	$r$
$\Delta M_{8LLEq}^{(e,e)}$	6	-35.1438 ( 514)	$1 \times 10^7$	80	1.62
$\Delta M_{8LLEq}^{(e,m)}$	6	0.0505 (16)	$1 \times 10^7$	40	
$\Delta M_{8LLEq}^{(m,e)}$	6	-0.9986 (17)	$1 \times 10^7$	120	
$\Delta M_{8LLEq}^{(m,m)}$	6	-0.1347 (2)	$1 \times 10^7$	80	
$\Delta M_{8LLFq}^{(e,e)}$	12	-100.5201 (458)	$4 \times 10^7$	220	1.33
$\Delta M_{8LLFq}^{(e,m)}$	12	0.3570 (19)	$1 \times 10^7$	100	
$\Delta M_{8LLFq}^{(m,e)}$	12	-2.4368 (41)	$1 \times 10^7$	140	
$\Delta M_{8LLFq}^{(m,m)}$	12	-0.2254 (3)	$1 \times 10^7$	100	
$\Delta M_{8LLGq}^{(e,e)}$	12	-38.1520 ( 399)	$1 \times 10^7$	80	1.09
$\Delta M_{8LLGq}^{(e,m)}$	12	-0.2662 ( 7)	$1 \times 10^7$	40	
$\Delta M_{8LLGq}^{(m,e)}$	12	-1.6144 (33)	$1 \times 10^7$	180	
$\Delta M_{8LLGq}^{(m,m)}$	12	-0.0957 (3)	$1 \times 10^7$	80	
$\Delta M_{8LLHq}^{(e,e)}$	6	64.5209 ( 879)	$1 \times 10^7$	80	1.19
$\Delta M_{8LLHq}^{(e,m)}$	6	-0.4527 (12)	$1 \times 10^7$	40	
$\Delta M_{8LLHq}^{(m,e)}$	6	0.3954 (39)	$1 \times 10^7$	160	
$\Delta M_{8LLHq}^{(m,m)}$	6	$-0.221 (91) \times 10^{-3}$	$1 \times 10^7$	80	
$\Delta M_{8LLIq}^{(e,e)}$	12	189.0518 (620)	$4 \times 10^7$	200	1.68
$\Delta M_{8LLIq}^{(e,m)}$	12	1.8726 ( 19)	$1 \times 10^7$	80	
$\Delta M_{8LLIq}^{(m,e)}$	12	2.0747 ( 37)	$1 \times 10^7$	200	
$\Delta M_{8LLIq}^{(m,m)}$	12	0.0719 ( 2)	$1 \times 10^7$	80	

TABLE XII: Numerical evaluation of diagrams of Set VI(f). The notation follows that of [42] with some modification and adaptation. The suffix  $p$  indicates insertion of  $\Pi_2$  in the photon lines connecting the muon line and the  $l-l$  loop.  $r = \Delta M_{8LLxp}/\Delta M_{8LLx}$ , where  $x = A, B, C, D$ , in column 6 is for comparison with the enhancement factor  $3K_\eta$  for set VI(f) discussed in Sec. III.

Integral	$n_F$	Value (error) including $n_F$	Sampling per iteration	No. of iterations	$r$
$\Delta M_{8LLAp}^{(e,e)}$	30	307.3206 (848)	$4 \times 10^7$	200	5.90
$\Delta M_{8LLAp}^{(e,m)}$	30	8.9175 ( 82)	$1 \times 10^7$	120	
$\Delta M_{8LLAp}^{(m,e)}$	30	2.9097 (118)	$1 \times 10^7$	100	
$\Delta M_{8LLAp}^{(m,m)}$	30	0.7878 ( 10)	$1 \times 10^7$	200	
$\Delta M_{8LLBp}^{(e,e)}$	60	-482.5729 (603)	$1 \times 10^8$	200	6.43
$\Delta M_{8LLBp}^{(e,m)}$	60	-16.0636 ( 78)	$1 \times 10^7$	120	
$\Delta M_{8LLBp}^{(m,e)}$	60	-13.7242 (121)	$2 \times 10^7$	100	
$\Delta M_{8LLBp}^{(m,m)}$	60	-1.7449 ( 12)	$1 \times 10^7$	280	
$\Delta M_{8LLCp}^{(e,e)}$	60	645.3472 (823)	$1 \times 10^8$	200	6.00
$\Delta M_{8LLCp}^{(e,m)}$	60	19.7833 ( 82)	$1 \times 10^7$	180	
$\Delta M_{8LLCp}^{(m,e)}$	60	30.4954 (125)	$2 \times 10^7$	240	
$\Delta M_{8LLCp}^{(m,m)}$	60	3.4824 ( 16)	$1 \times 10^7$	300	
$\Delta M_{8LLDp}^{(e,e)}$	30	-252.4292 (616)	$4 \times 10^7$	200	6.67
$\Delta M_{8LLDp}^{(e,m)}$	30	-8.4527 ( 66)	$1 \times 10^7$	80	
$\Delta M_{8LLDp}^{(m,e)}$	30	-1.1736 ( 86)	$1 \times 10^7$	140	
$\Delta M_{8LLDp}^{(m,m)}$	30	-0.4074 ( 8)	$1 \times 10^7$	200	

TABLE XIII: Numerical evaluation of diagrams of Set VI(i). The notation follows that of [42] with some modification and adaptation. The suffix  $q$  refers to insertion of  $\Pi_2$  in radiative corrections to the  $l-l$  loop.  $r = \Delta M_{8LLxp}/\Delta M_{8LLx}$ , where  $x = A, B, C, D$ , in column 6 is for comparison with the enhancement factor  $K_\eta$  for set VI(i) discussed in Sec. III.

Integral	$n_F$	Value (error) including $n_F$	Sampling per iteration	No. of iterations	$r$
$\Delta M_{8LLAq}^{(e,e)}$	10	29.6915 (199)	$1 \times 10^7$	80	0.57
$\Delta M_{8LLAq}^{(e,m)}$	10	0.0914 ( 3)	$1 \times 10^7$	40	
$\Delta M_{8LLAq}^{(m,e)}$	10	0.4867 (30)	$1 \times 10^7$	100	
$\Delta M_{8LLAq}^{(m,m)}$	10	$0.8068 (93) \times 10^{-2}$	$1 \times 10^7$	140	
$\Delta M_{8LLBq}^{(e,e)}$	20	-81.3369 (946)	$1 \times 10^7$	95*	1.08
$\Delta M_{8LLBq}^{(e,m)}$	20	-1.2816 (26)	$1 \times 10^7$	100	
$\Delta M_{8LLBq}^{(m,e)}$	20	-4.6043 (69)	$1 \times 10^7$	138	
$\Delta M_{8LLBq}^{(m,m)}$	20	-0.4926 (8)	$1 \times 10^7$	200	
$\Delta M_{8LLCq}^{(e,e)}$	20	71.0664 (409)	$1 \times 10^7$	80	0.66
$\Delta M_{8LLCq}^{(e,m)}$	20	0.7624 ( 7)	$1 \times 10^7$	40	
$\Delta M_{8LLCq}^{(m,e)}$	20	8.5729 (59)	$1 \times 10^7$	160	
$\Delta M_{8LLCq}^{(m,m)}$	20	0.5664 (4)	$1 \times 10^7$	100	
$\Delta M_{8LLDq}^{(e,e)}$	10	-43.7735 (449)	$1 \times 10^7$	80	1.16
$\Delta M_{8LLDq}^{(e,m)}$	10	-0.6699 (14)	$1 \times 10^7$	60	
$\Delta M_{8LLDq}^{(m,e)}$	10	-0.2587 (42)	$1 \times 10^7$	100	
$\Delta M_{8LLDq}^{(m,m)}$	10	-0.0551 (5)	$1 \times 10^7$	140	

TABLE XIV: Numerical evaluation of diagrams of Set VI(j) contributing to the muon g-2. In the superscript  $(a, b)$ ,  $a$  and  $b$  refer to the external and internal light-by-light-scattering loop, respectively. Last 4 lines with superscript  $(m, m)$  are mass-independent so that they are identical with the contributions to the electron g-2.

Integral	$n_F$	Value (Error) including $n_F$	Sampling per iteration	No. of iterations
$X6J_a^{(e,e)}$	24	0.57928 (0.01386 )	$1 \times 10^8, 1 \times 10^9$	100, 294
$X6J_b^{(e,e)}$	12	-16.91235 (0.00630 )	$1 \times 10^8, 1 \times 10^9$	100, 100
$X6J_c^{(e,e)}$	12	-23.00801 (0.00777 )	$1 \times 10^8, 1 \times 10^9$	100, 160
$X6J_d^{(e,e)}$	6	15.38181 (0.00388 )	$1 \times 10^8, 1 \times 10^9$	100, 87
$X6J_a^{(e,m)}$	24	4.75211 (0.00609 )	$1 \times 10^8$	105
$X6J_b^{(e,m)}$	12	-0.84570 (0.00112 )	$1 \times 10^8$	100
$X6J_c^{(e,m)}$	12	-5.96339 (0.00157 )	$1 \times 10^8$	190
$X6J_d^{(e,m)}$	6	0.88153 (0.00046 )	$1 \times 10^8$	220
$X6J_a^{(m,e)}$	24	-2.06921 (0.00549 )	$1 \times 10^8$	100
$X6J_b^{(m,e)}$	12	-3.75200 (0.00232 )	$1 \times 10^8$	100
$X6J_c^{(m,e)}$	12	1.64453 (0.00162 )	$1 \times 10^8$	200
$X6J_d^{(m,e)}$	6	3.80656 (0.00138 )	$1 \times 10^8$	130
$X6J_a^{(m,m)}$	24	-0.22601 (0.00143 )	$1 \times 10^8$	180
$X6J_b^{(m,m)}$	12	-0.69698 (0.00065 )	$1 \times 10^8$	100
$X6J_c^{(m,m)}$	12	-0.02753 (0.00053 )	$1 \times 10^8$	170
$X6J_d^{(m,m)}$	6	0.72170 (0.00037 )	$1 \times 10^8$	100

TABLE XV: Numerical evaluation of diagrams of Set VI(k) contributing to the muon g-2. The superscript  $e$  ( $m$ ) indicates that the lepton loop  $\Lambda_6$  is the electron (muon) loop. The latter is mass-independent so that it is identical with the contribution to the electron g-2.

Integral	$n_F$	Value (Error) including $n_F$	Sampling per iteration	No. of iterations
$X6k_a^{(e)}$	10	50.35921 (0.01998 )	$1 \times 10^8, 1 \times 10^9$	500 , 150
$X6k_b^{(e)}$	10	1.72669 (0.01786 )	$1 \times 10^8$	400
$X6k_c^{(e)}$	20	7.81330 (0.02038 )	$1 \times 10^8$	300
$X6k_d^{(e)}$	20	20.67840 (0.03758 )	$1 \times 10^8$	100
$X6k_e^{(e)}$	10	-0.19466 (0.01045 )	$1 \times 10^8$	300
$X6k_f^{(e)}$	10	1.75890 (0.02374 )	$1 \times 10^8$	230
$X6k_g^{(e)}$	20	-0.02607 (0.01797 )	$1 \times 10^8$	200
$X6k_h^{(e)}$	10	-0.69054 (0.00750 )	$1 \times 10^8$	100
$X6k_i^{(e)}$	10	15.69736 (0.01595 )	$1 \times 10^8$	200
$X6k_a^{(m)}$	10	-0.56022 (0.00301 )	$1 \times 10^8$	100
$X6k_b^{(m)}$	10	0.30282 (0.00085 )	$1 \times 10^8$	100
$X6k_c^{(m)}$	20	-0.32547 (0.00114 )	$1 \times 10^8$	100
$X6k_d^{(m)}$	20	0.82380 (0.00084 )	$1 \times 10^8$	100
$X6k_e^{(m)}$	10	-0.17188 (0.00053 )	$1 \times 10^8$	100
$X6k_f^{(m)}$	10	0.30329 (0.00088 )	$1 \times 10^8$	100
$X6k_g^{(m)}$	20	-0.94843 (0.00067 )	$1 \times 10^8$	100
$X6k_h^{(m)}$	10	-0.13877 (0.00018 )	$1 \times 10^8$	100
$X6k_i^{(m)}$	10	1.39510 (0.00069 )	$1 \times 10^8$	100